DETERMINATION OF NEURONAL MORPHOLOGY IN SPINAL MONOLAYER CULTURES

THESIS

Presented to the Graduate Council of the
University of North Texas in Partial
Fulfillment of the Requirements

For the Degree of

Master of Science

By

Richard DeLaGarza II, B. S.

Denton, Texas

May, 1989

GW6

De La Garza, Richard II, Determination of Neuronal Morphology in Spinal Monolayer Cultures. Master of Science (Neurophysiology), May 1989, 107 pp., 22 figures, 3 tables, 30 illustrations, literature cited, 77 titles.

The objective of the completed research was to characterize the morphology of individual neurons within monolayer networks of fetal mouse spinal tissue via intraperikaryal injections of horseradish peroxidase (HRP). Thirty labelled neurons were reconstructed via camera lucida drawings and morphometrically analyzed.

From the database established in this study, it is now possible to generate certain predicted values for the portion of a neuron's dendritic domain that is not visible in culture. The dendritic field is shown to increase with increasing somal diameter, total dendrite length increases linearly with increasing primary dendrite diameter, and the greatest percentage of total dendrite length is found approximately 120-200 μm from the soma.

ACKNOWLEDGEMENTS

I wish to thank Linda Czisny and Janet Douglass who provided the high quality cell cultures which made this research possible. I also wish to express my appreciation to Dr. Michael Droge and Texas Woman's University for the use of their Video Image Analysis System. Finally, I would also like to express my gratitude to Mary Hightower and Jen Lucas for their advice and continuous support throughout the course of the research.

TABLE OF CONTENTS

LIST OF TABLES

LIST OF ILLUSTRATIONS

LIST OF ILLUSTRATIONS cont.

Introduction and Project Objectives

Multielectrode recording from monolayer neuronal networks in culture has been utilized in order to disclose basic principals of network architecture and function. A continual concern is the necessity of mapping cell circuitry in small monolayer cultures so that electrical activity can be correlated with network structure. The morphological features of monolayer networks are not well defined because of the great complexity of even low density cell cultures. Circuit mapping (i.e., the determination of how cells are interconnected) is complicated by fasciculation of axons and complex "contour following" of axons along dendrites and perikarya and by the lack of reliable techniques for showing synapses with light microscopy (Gross and Hightower, 1987). While it is assumed that there is substantial axonal and dendritic growth and arborization in small monolayer cultures, there is no available data which assesses the structural detail present. The determination of average dendrite and axonal domains for specific cell types would be of great value to the planning of network simplification strategies in culture as well as to the interpretation of multielectrode recordings.

Minicultures are unique 1-2 mm diameter monolayer cultures developed in this laboratory. Their purpose is to reduce the complexity of the cell circuitry by restricting neurite growth to a given adhesion area. Multielectrode recording with fixed photoetched electrode patterns presently allows only a random sampling of network activity. It is essential that morphological domains be investigated to determine how far from a perikaryon an axon may cross a recording electrode and how large an input field is generated by the dendrites.

Specific Aims

The objective of the completed research was to characterize the morphology of individual neurons within monolayer networks of fetal mouse spinal tissue in order to determine differences and similarities between *in vitro* and *in vivo* networks. In addition, the trends that exist between cell body size, shape, and proximal dendrite size and number with the overall axonal and dendritic domains formed by these cells was investigated. Such a correlation would be very useful to establish the size of the input and output fields of cells in monolayer cultures. This is of special significance for multimicroelectrode analyses where the fine dendritic branches or axonal arborizations can not be clearly distinguished in the living state with phase contrast or differential interference contrast microscopy.

The specific aims of this project were: (1) to correlate cell size with total axon length, (2) to correlate cell size with total dendrite length, (3) to correlate cell size with axonal and dendritic domains, (4) to determine the average distance from the soma where the greatest percentage of dendritic segments are located and (5) to determine if the 3/2 rule applies to dendritic branching in culture. In addition it was the goal of this study to identify any parameter, observable with light microscopy, that could be used to predict other cell features not distinguishable in living cell cultures.

Introduction to Intracellular Staining Methods

Intracellular staining methods through microelectrodes allows clear unequivocal identification of neurons after electrophysiological recordings have been made. In terms of morphological detail, intracellularly-stained neurons are known to provide as much and usually more morphological detail than nerve cells impregnated with the Golgi method (Bishop and King, 1982). A primary advantage of intracellular injection is the specificity of labelling which can be obtained. In the Golgi technique, multiple nerve cells may be stained, making it difficult to completely identify the processes of an individual cell. With intracellular staining, only one neuron is stained in a specific area. Thus the neuron can be completely visualized

and reconstructed at light microscopic levels. In addition, the intracellular method greatly facilitates comparisons of light microscopic images with subsequent electron micrographs (Jankowska et al., 1976; Muller and McMahan, 1976; Cullheim et al., 1977; Christian and Ebner, 1978; King and McCrea 1978). Consequently, the ultrastructural features of a specific soma , dendrite, axon, or axon collateral can be determined and compared with that neuron's physiological properties. The major application of the intracellular method is to analyze the local circuitry of the central nervous system (Cullheim and Kellereth, 1976; Kitai et al., 1976; Snow et al., 1976; Cullheim et al., 1977; Bishop et al., 1979a; 1980a, b; Preston et al, 1980; Chang et al., 1980; Deniau et al, 1980; and Gobel et al, 1980).

Intracellular Application of HRP

Analysis of neurons subsequent to intracellular application of HRP results in transport of the enzyme throughout the soma, dendrites, dendritic spines, axons and fine axon collaterals. The most important advantage associated with the use of HRP is that it provides the most detailed view of a neuron that can presently be obtained. It is well known that HRP gives a more complete view than the Golgi method which has been shown to miss entire dendritic systems (Somogyi and Smith, 1979; Brown and Fyffe, 1981). One main disadvantage of HRP is the occasional

leakage of the enzyme from the tip of the microelectrode resulting in an extracellular deposit of reaction product. This stains the surrounding area and makes it difficult to distinguish the very fine processes of a dendritic tree. A second disadvantage of the HRP method is related to the high specificity of labelling that occurs, disallowing neurons to be stained in close proximity to each other. Although it may be advantageous to sometimes stain cells close to one another, it often becomes impossible to differentiate between the processes belonging to the two cells. Finally, HRP may not always fill the tips of small axonal processes and therefore it is not possible to assess the complete axon with its subsequent branches.

Extracellular Application of HRP

After extracellular application, HRP gains entry into neurons through a process of endocytosis. The membrane-delimited endocytotic vesicles which contain the enzyme are then transported along the labelled neural processes. While the HRP molecule is not itself visible, readily detectable reaction product is obtained by the enzymatic action at the site of administration as well as at the sites of transport (Mesulam, 1982).

Endocytosis occurs along the entire plasmalemma. The process may be described as an invagination of the walls of the surface membrane. The resultant vacuole is often a

coated vesicle approximately 100 nm in diameter. Endocytosis occurs throughout the membrane of neurons, including perikarya, dendrites, axons, and their terminals (Brightman, 1965; Broadwell and Brightman, 1979; LaVail and LaVail, 1974; Turner and Harris, 1974; Waxman and Pappas, 1969).

Demonstration of Neural Connections With HRP

Conclusive demonstration of neural connections by means of transported HRP was not accomplished until the experi-ments of Kristensson and Olsson in 1971. They reported that the retrograde transport of intramuscularly administered HRP could be readily demonstrated in spinal cord tissue fixed and processed with diaminobenzidine (DAB) according to Graham and Karnovsky (1966). Subsequent experiments by LaVail and LaVail (1974) and Turner and Harris (1974) introduced HRP histochemistry as a major method for tracing neural connections.

Methods of Administration of HRP

Free HRP can be administered in the form of aqueous solutions, solids, gels, or pastes. Aqueous solutions are most commonly used. While a few investigators have used pressure injection as a means to administer HRP (Sakai and Woody, 1978; Sakai et al., 1978, Nahvi et al., 1980; Ribak et al, 1980), most commonly a constant current source is applied to the electrode. Such microiontophoretic injections are methods which allow minute amounts of enzyme

to be deposited (Lynch et al., 1973; Graybiel and Devor, 1974).

Markers for Detecting Distribution of HRP

Four approaches are available for detecting the distribution of HRP in neural tissue. One approach is based on covalent binding of the HRP molecule to a fluorescent substance (Hanker et al., 1976; Norden et al., 1976). A second approach includes immunohistochemical detection of the enzyme through the formation of HRP-anti-HRP complexes (Vacca et al., 1975; Sofroniew and Schrell, 1980). A third alternative is to attach a radioactive label to the HRP molecule and to trace the distribution of the tissue-bound enzyme by autoradiography (Geisert, 1976). The fourth and most widely incorporated strategy, is to use the enzymatic activity of the HRP itself to produce a visible reaction product.

Anterograde versus Retrograde Transport of HRP

Much of the anterograde transport occurs within 50-80 nm membranous vesicular structures. Retrograde transport, which is similar in dynamics, occurs within larger membranous vesicular bodies (LaVail et al., 1980; Teichberg et al., 1975; Tscihita and Ishikawa, 1980). Both types of transport are energy dependent and can be blocked by metabolic inhibitors (Ochs and Worth, 1978). It is

important to mention that experimenters suggest that microtubules have a decisive role in fast anterograde and retrograde vesicular transport (LaVail and LaVail, 1974; Mesulam and Mufson, 1980; Ochs and Worth, 1978; Schwartz, 1979; Smith, 1971). Furthermore, uptake (and therefore greater subsequent transport) is coupled to neural activity and can be enhanced when neural activity in that area is increased (Broadwell and Brightman, 1979; Litchy 1973; Nishino et al., 1979). Additionally, experimenters have found that transport of HRP occurs at a rate of 84-113 mm/day in the retrograde direction (LaVail and LaVail, 1974) and 288-432 mm/day in the anterograde direction (Mesulam and Mufson, 1980).

Histochemical Sensitivity: A Key Factor

The sensitivity of the histochemical procedure was conclusively shown to influence the extent of the neural connections demonstrated with HRP (Mesulam, 1976). It was demonstrated that excessive fixation could fail to produce detectable levels of reaction product at the sites that contained the transported HRP (Mesulam and Rosene, 1979; Rosene and Mesulam, 1978). Initially, experimenters were led to assume absence of reaction product as an absence of transport. Several procedures were subsequently introduced which improved histochemical sensitivity by modifying the parameters of fixation and enzymatic incubation (Malmgren

and Olsson, 1978; Mesulam, 1976a; Mesulam and Rosene, 1977; Rosene and Mesulam, 1978; Streit and Reubi, 1977).

Completeness of Axonal Labelling

Besides studying the local circuitry, the intracellular administration of HRP can also be used in axonal tracing studies. This approach provides information on the course and distribution of axons (Cullheim and Kellereth, 1976; Snow et al., 1976; McCrea et al., 1976, 1977; Bishop et al., 1979a, b; Mason and Robson, 1979; Robson and Mason, 1979; Preston et al., 1980; Deniau et al., 1980). The major limitation of using this intracellular staining method for tracing axons is that the enzyme does not always label the axon to its termination.

When HRP is administered directly into the perikaryon, the resultant staining obtained with the DAB procedures yields a diffuse labelling of virtually the entire dendritic tree and of the initial axon segment. Ultrastructural examination after intracellular HRP injection indicates that the reaction product is distributed diffusely within the cytoplasm and that it lines the plasma membrane, the perikaryon, mitochondria, and other membrane-delimited organelles. Only a limited length of the axon can be labelled following the intraperikaryal administration of HRP. It has therefore been concluded by Mesulam (1976) that

the axonal labelling following direct intraperikaryal injection of HRP occurs mostly through passive diffusion.

It appears that survival times play a decisive role in determining the degree of staining for the neuron. The major limitation encountered here is that insufficient survival time (after injection) will limit the ability to identify axons that travel over long distances. Increases in sensitivity of the histochemical procedures has not proven helpful in this case.

Electrophysiological Recordings

Large neurons do not survive in culture as well as smaller cell bodies. In addition, vibrations in the electrode are not dampened by surrounding tissue. Finally, tip diameters are generally larger than what is optimal for electrophysiological recordings because the HRP can easily block the electrodes. These factors all contribute to membrane damage which often reduce the membrane potential to 20 mv. Although this is unacceptable for electrophysiological studies it has been noted that the neuron can still be injected and recovered in an apparent normal morphological condition. In fact, no statistically significant correlation was found between the amplitude of the preinjection potential the quality of the staining (Bishop, 1980b).

Neuron Morphology Through Golgi Techniques

For years researchers have provided substantial detail of the somatodendritic characteristics of neurons in many areas of the central nervous system using the Golgi technique (e.g., Ramon y Cajal, 1911; Scheibel and Scheibel, 1955; Fox et al, 1967; 1971/1972a, b; Chan-Palay, 1971; 1977; Kemp and Powell, 1971; Bowman and King, 1973; Palay and Chan-Palay, 1974; DiFiglia et al., 1976; Gwynn et al., 1977). Unfortunately, the Golgi technique is notoriously difficult and has many disadvantages that render it undesirable. Some neuronal types do not take up the stain at all and even those that do may show incomplete labelling of the dendrites and axon therefore lending to false interpretations of dendritic and axonal fields.

Commonly Used Intracellular Markers Other Than HRP

Two commonly used fluorescent stains include the procion dyes and a naphthalimide dye, lucifer yellow. Procion yellow is the best of the procion dyes for intracellular staining (Brown and Fyffe, 1981). Useful data may be obtained with this technique, especially with regard to the ultrastructure of the cell body and proximal dendrites and the contacts that they receive. A major advantage of procion yellow is the relative ease with which the technique can be used because no histochemical processing such as with HRP is required. The major

disadvantage of procion yellow is that it does not give a complete picture of the cell's dendritic tree nor complete filling of the axon and axon collaterals. On the other hand, lucifer yellow, provides a more detailed picture than procion yellow as finer processes are revealed, and more of the axon and its branches can be seen. Again, however, the major disadvantage encountered is the incomplete labelling that may occur as with procion yellow.

Cobaltous chloride is another substance currently used as an intracellular marker for neurons primarily with invertebrates and amphibians (Gillete and Pomeranz, 1973a; Szekely, 1976; Szekely and Kosaras, 1976). Detailed labeling of a neuron has been obtained with this method but it has several disadvantages. Among these are (1) cobalt is toxic to the neuron and alters the physiological response following the impalement, (2) cobalt tends to block the electrode during iontophoresis, and (3) cobalt must be reacted within 30 minutes of the impalement or a precipitate will not form. This drastically limits the number of neurons which can be labelled per experiment.

Materials and Methods and Experimental Protocol

Cell Culture

Spinal cords from 13 to 15 day old mouse embryos were dissociated and cultured according to the method of Ransom et al (1977) as modified by Gross and Lucas (1982). Cultured neuronal monolayer networks were obtained from the cell culture staff in this laboratory. A short description of the culture procedures is included in this section for the convenience of the reader.

The pregnant mice were killed by cervical dislocation during CO_2 narcosis. The CO_2 produced unconsciousness without the possible tissue damage that may result from chloroform or ether anesthesia. The uterus was removed and placed in a 100 mm petri dish containing cold sterile D1SGH solution. D1SGH is a saline solution used for maintenance of the tissue before it is separated into single cells. Embryos were separated and transferred to a 60 mm petri dish containing D1SGH. Each spinal cord took about one minute to remove. The D1SGH solution of 1 liter was made up of 50 ml of 20x concentrated Puck's D1 salt solution, 6 g glucose, 15 g sucrose per liter, and 10 mM HEPES buffer, pH 7.3. The complete solution was adjusted to 320 mOsm with water.

Following dissection, four to five spinal cords were placed in an empty sterile 60 mm petri dish and minced with scalpels until the mass of the tissue appeared almost gelatinous. The tissue was taken up in D1SGH solution and transferred to a centrifuge tube using a siliconized Pasteur pipette (all glass pipettes that are used for pipetting tissue were silconized to prevent the tissue from sticking to the glass surface). The tissue fragments were centrifuged for approximately two minutes at 800 RPM. Afterward, the supernatant was discarded. Three ml of 0.25% trypsin + DNAase (0.5 mg/ml) was added to the tissue pellet. The pellet was resuspended and the solution and tissue were transferred to a 60 mm tissue culture dish. The dish was placed in a 37°C, 10% CO_2 incubator for 20 minutes. The trypsin activity was stopped at 20 minutes by pipetting the tissue/trypsin solution into 6 ml of MEM 10/10. The tube was centrifuged for 1-2 minutes at 700 RPM to facilitate the sedimentation of the tissue. Afterward, the tissue was removed by means of a Pasteur pipette, minimizing uptake of supernatants as much as possible, and placed into another 15 ml centrifuge tube. The remaining supernatant was discarded. Two ml of MEM 10/10 was added to the tissue and triturated using a siliconized Pasteur pipette. The solution was triturated 15 times. The tissue fragments were allowed to settle to the bottom of the tube leaving single cells in the upper volume of the fluid. This upper layer of

the medium was carefully drawn off and placed into a separate tube. Another 1-2 ml of MEM 10/10 was added to the tissue fragments and triturated again with a Pasteur pipette of a slightly narrowed opening. The fragments were allowed to settle to the bottom and the supernatant of single cells was drawn off and pooled with previously extracted single cells. Another 1-2 ml of MEM 10/10 was added to the tissue fragments and triturated a final time using a Pasteur pipette of an even narrower opening. The layer of single cells was again removed and placed with the single cell pool. The cell pool was gently triturated to obtain a homogeneous mixture. Cells were counted with a hemacytometer and diluted to one million per milliliter. Cells were seeded at 800,000 per 22 mm x 40 mm coverslip.

Care of neuronal cultures was as follows: DAY 0: seeding, MEM 10/10. DAY 1: medium containing unattached cells and debris was removed from the cultures and replaced with fresh MEM 10/10 (complete medium change). DAY 4 or 5: the cultures received a complete medium change replacing the MEM 10/10 with MEM 10 horse serum. DAY 6 or 7: When the glial carpet was confluent it was treated with fluorodeoxyuridine/uridine (FdU) to retard non-neuronal cell division (Ransom, et al 1977). At the time of application 1 ml of FdU stock was added to 30 ml of MEM 10 and a complete medium change was performed. The FdU treatment lasted approximately 48 hours. DAY 8 or 9; The FdU was removed and

a complete medium change was performed replacing the medium with fresh MEM 10. The final molar concentrations of FdU and uridine in culture were 5.4×10^{-5} and 1.4×10^{-4} respectively.

For maintenance purposes, routine feeding was begun three to four days after the FdU removal. Cultures were fed every three to four days depending on cell density and medium volume. As cell density increased, feeding frequency was also increased. As well, surface area to volume ratios were monitored and cell feeding was delayed when a greater volume existed in relation to surface area. When the medium on the cells began to turn more orange than peachy-red, the culture was fed. Partial medium changes were performed by removing one-third to one-half of the medium on the culture and replacing it with an equal volume of MEM 10.

Cultures 4 to 5 weeks of age were selected for experiments. Microscopic observation determined use if minimal amount of cell aggregation was observed, and if a good sample of well developed, large neurons was present.

Injection

Electrode Preparation

Electrodes were pulled using the David Kopf 750 vertical needle/pipette puller. Microprocessor control of parameters in the pulling sequence coupled with the length of the gravity fall and solenoid pull and adjustable heater

filaments allowed for variation of pipettes. Tip diameters of <1 μm were sought and those with impedance values of 60 - 100 MΩ were used. Newly pulled electrodes were visually inspected by placing them in a small section of modeling clay pressed onto a microscope slide. The tip configuration, shape of the taper, and shank length were evaluated. If the pipette appeared useable, an impedance measurement was performed. Impedances were measured using the World Precision Instruments (WPI) Volt-Ohmmeter, Model F-29. At this point, a pipette which was visually inspected and approved, and which had a reasonable resistance, was selected for upcoming experiments and the program which produced that pipette was stored.

Pipette glass was obtained from WPI and had the following specifications: 1 barrel, with filament, 1.0 mm outer diameter, 0.58 mm inner diameter, and 6 inch length. The 6 inch length allowed two pipettes to be pulled per glass rod in contrast to the less expensive 4 inch glass which allowed only one pipette to be pulled per rod. The pipette glass is borosilicate and two different lot numbers, 10242-11F and 107599-04G, were used during the course of the research.

Impalement

Prior to filling, pipettes were again visually inspected and those suitable for use were momentarily dipped

into a solution of Antispread M 2/200 - ultra clean, an epilamisation agent (lot number A351232.01, Etsyntha Chemie, West Germany). This anti-adhesive agent lowers the surface tension of the electrode glass, and helps reduce damage and distortion to the tissue by preventing the microelectrode from sticking to cell membranes. It has been shown to increase successful impalements by about 30% (Jarvilehto et al., 1986). Fine tipped pipettes were filled with the 4% HRP solution using a 33 gauge, 2 inch long Hamilton microsyringe. Care was taken to eliminate air bubbles by tapping the pipette with the tip pointed downward. The stem of the pipette was positioned into a WPI MEH-1S micro-electrode holder half cell which had been filled with the same HRP solution. The 2 mm diameter stainless steel receptacle of the microelectrode holder connects directly to the input of the WPI dual microprobe system. An Ag/AgCl half cell, molded into the holder, provided the interface to the microelectrode electrolyte. The outside of the holder, around the gasket, was carefully dried with a tissue to prevent any solution from creeping down the electrode into the culture dish. The pipette was advanced using a WPI DC 3000L motorized micromanipulator which controls x, y, and z axis movements at specified increments. The WPI Dual Microprobe System KS-700 was used for monitoring the intracellular potential, application of current, and

occasionally for penetration by "ringing" with the capacity compensation control.

All experiments were performed upon a vibration isolation table (Technical Manufacturing Corporation, Model 63-484). A continuous stream of dry 30% CO_2/70% air was passed across the 10x lens objective by means of a special plastic sleeve developed in this laboratory to maintain the culture pH at approximately 7.4, and to prevent condensation on the objective. During the experiment, 250 µl of distilled water was added to the culture dish medium every 30 minutes to compensate for evaporation and to maintain normal osmolarity of the medium (Lucas et al, 1985). The cells were maintained between 35°C and 37°C during experimentation.

Once the pipette was placed into the medium, prior to impalement, the dual microprobe system was zeroed. Simultaneously, recordings were documented through use of a Linseiss TYP-7045 chart recorder. The pipette was slowly advanced to just above the cell to be injected, the stage of the microscope was lowered by defocusing, the pipette was lowered into the focal plane, and the stage was returned upward by fine focusing. A small dimple was usually observed on the cell accompanied by a slight positive shift of the zeroed chart recorder indicating that the cell was ready to be penetrated (Fig. 1). Penetration was most commonly achieved by a quick but gentle jab of the

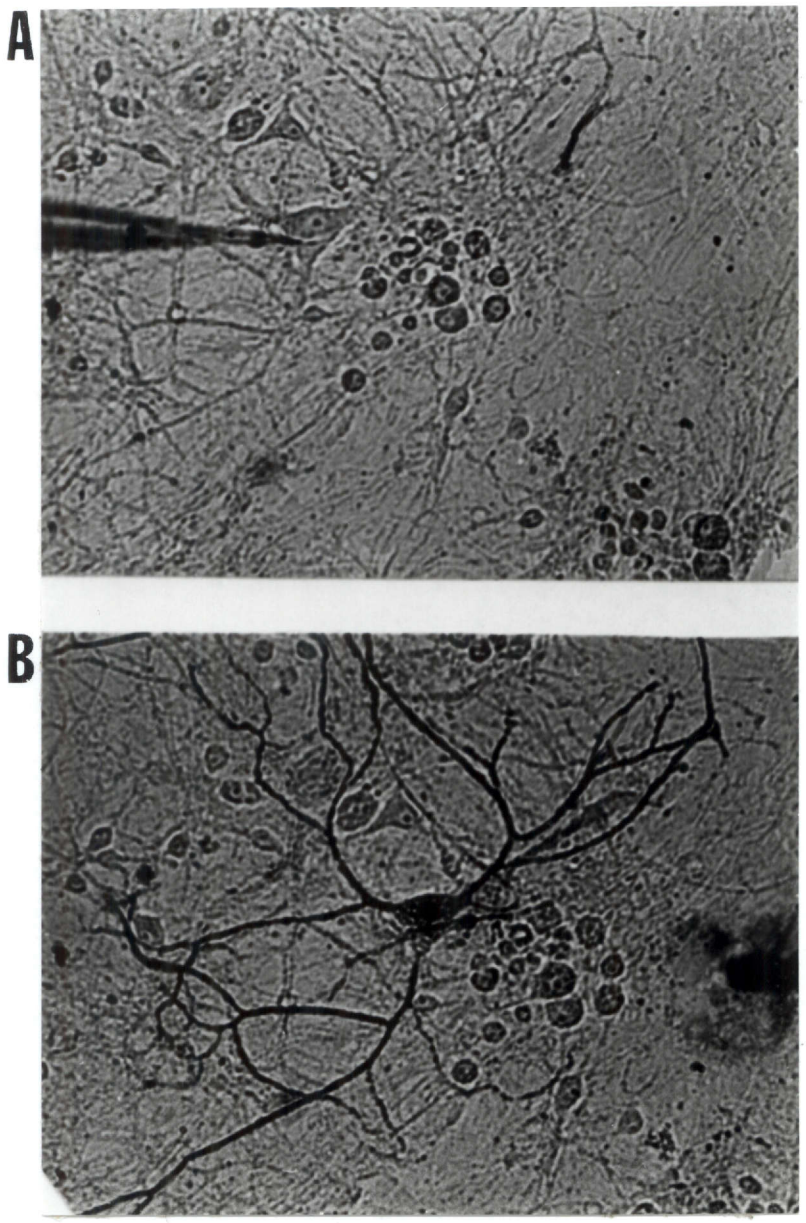

Figure 1. Photographs of a typical pyramidal shaped neuron preinjection (A), with electrode upon neuron, and postinjection (B), after transport of HRP and histochemical processing.

microscope stage opposite to the direction of pipette entry. Alternatively, penetrations were sometimes made using the capacity compensation of the dual microprobe system, which created a small vibration at the tip of the electrode and consequent entry. Upon impalement, and once a steady resting potential had been established, the neuron was injected with HRP solution using low intensity depolarizing current of 10-15 nA for 3-5 minutes. Greater intensity currents, 20-25 nA, were also sometimes used for larger cells.

Pressure injection using the WPI A-1400 Nanoliter pump was attempted but was later abandoned due to its many shortcomings. These are discussed in detail in the discussion section of the thesis.

Solution Preparation

Four stock solutions were used to make the injection, fixation, and reaction solutions. These included 0.1 M phosphate buffer (pH 7.4), 0.1 M Tris HCl buffer (pH 7.4), 0.2 M KCl - 0.05 M Tris buffer (pH 8.6), and 0.01 % Hydrogen Peroxide - 0.1 M Phosphate buffer (pH 7.4). Preparation of 0.1 M phosphate buffer was as follows: 1.2 grams of monobasic sodium phosphate (mwt. 120) was added to 5.7 grams of dibasic sodium phosphate (mwt. 142) and deionized water was added to yield a total volume of 500 ml. The pH was brought to 7.4 and the solution was stored in the

refrigerator. The 0.1 M Tris HCl buffer solution was prepared in a 250 ml quantity as follows: 3.95 grams of Tris HCl Buffer (158 daltons) was added to de-ionized water to yield a total volume of 250 ml. The pH was brought to 7.4 and the solution was stored in the refrigerator. The 0.2 M KCl - 0.05 M Tris Buffer solution was prepared as follows: 3.73 grams of KCl (mwt. 74.55) was added to 1.98 grams Tris buffer (mwt. 158) and deionized water was added to yield a total volume of 250 ml. The pH was brought to 8.6 and the solution was stored in the refrigerator. The 0.01% hydrogen peroxide - 0.1 M phosphate buffer was prepared as follows: 0.8 ml of 3% hydrogen peroxide was added to 0.1 M Phosphate buffer to yield a total volume of 250 ml. The pH was brought to 7.4 and the solution was stored in the refrigerator.

The injection solution of 4% horseradish peroxidase (HRP) in 0.2 M KCl - 0.05 M Tris Buffer was prepared in a 300 µl quantity. The HRP was ordered from Sigma Chemical Company of St. Louis, Montana as peroxidase (Donor: hydrogen-peroxide oxidoreductase EC 1.11.1.7) from horseradish, Type VI. The lot number of the chemical was 125F-9645 and was used throughout the course of this study. The chemical was stored desicated below 0° C and was allowed 30 minutes to warm up to room temperature prior to removing the vacuum. Three mg of HRP were weighed out and added to

300 µl of 0.2 M KCl - 0.05 M Tris Buffer. The solution was refrigerated and used within one hour.

The fixation solution of 1.25% glutaraldehyde in 0.1 M phosphate buffer was prepared as follows: 0.75 ml of 25% glutaraldehyde was added to 14 ml of 0.1 M phosphate buffer to make 15 ml. The pH was brought to 7.4 and the fixative was stored in the refrigerator. The solution was not used if it was more than 24 hours old due to deterioration of the glutaraldehyde. A combination of 1.25% glutaraldehyde/1% paraformaldehyde was initially used for fixation but was later abandoned due to the increased difficulty in preparation, and suggestions made by literature that some concentrations of paraformaldehyde are thought to result in less HRP reaction product (Kim and Strick 1976, Malmgren and Olsson 1978).

The reaction solution of diaminobenzidine in 0.01% hydrogen peroxide - 0.1 M phosphate buffer was prepared in a 30 ml quantity. The chemical, 3, 3′ diaminobenzidine tetrahydrochloride , was ordered from Sigma Chemical Company and only lot number 76F-3655 was used during the course of the research. Eight mg of DAB (mwt. 360.1) was added to 30 ml of 0.01% hydrogen peroxide in 0.1 M phosphate buffer. The solution was filtered as needed, stored in the refrigerator, and used within one hour.

Experimental Protocol

The following procedure was established for intracellular HRP injection and histochemical processing: (1) injection solution; 4% HRP, Sigma, Type VI, in 0.2 M KCl- 0.05 M Tris Buffer (pH 8.6); (2) impaling of cells, at 37°C, with minimum of one hour allowed for transport; (3) fixation and rinses: 1.25% glutaraldehyde in 0.1 M phosphate buffer (pH 7.6) for 15 minutes, followed by two separate rinses including 15 minutes in 0.1 M Tris-HCl buffer (pH 7.6), and a 5 minute rinse of 0.1 M phosphate buffer (pH 7.3); (4) reaction solution: diaminobenzidine (DAB) in 0.01% hydrogen peroxide and 0.1 M phosphate buffer (2-3 mg DAB per 10 ml buffer) was applied for at least one hour; (5) dehydration: application of each of the following solutions for a period of one minute each; 70% EtOH, 95% EtOH, 100% MeOH/50% Xylene, and 100% Xylene; (6) mounting: the coverglass was removed from the culture dish, inverted, and was then mounted onto a clean microscope slide using 4 to 5 drops Permount solution.

Morphological Reconstruction

Labeled neurons were relocated with light microscopy and were evaluated for completeness of filling by appearance. Some neurons, which were damaged upon penetration or exit, had cell bodies which were diffusely stained but showed no transport of the enzyme. Other cells,

showed obvious incomplete labeling due to insufficient current application, or the neuron was damaged during the injection process. These cells were not included in the data pool.

Labeled neurons were reconstructed via camera lucida drawings. Different size pens were used to accurately represent differences in the diameters of various portions of the neuronal processes. The cell soma was traced first and was followed by a tracing of the primary dendrites. Efforts were made to represent significant differences in diameter of the dendritic processes (secondary and tertiary dendrites) yet the use of even a 0.5 mm pencil lead proved insufficient after a certain point. Reconstructions were made on an Olympus IMT inverted microscope through a 5x drawing tube apparatus and the 20x magnification of the microscope objective onto high quality bond paper. The subsequent total magnification of the drawing was 100x.

Statistical Analysis

Statistical analysis of individual neurons was accomplished through the use of the Zeiss Videoplan II Image Analysis System. Analysis first included a measurement of the perikarya area, diameter, and perimeter. The area of the cell body was drawn by a smooth line that closely followed the cell border but excluded the sharply tapering 'hillocks' of emerging dendrites or axon

(Zwaagastra and Kernell, 1981). The image analysis system was also used to determine the length of the dendrites and axon for each cell. Most importantly, these statistics allowed for the evaluation of these factors; (1) the total length of primary dendrites and subsequent branches, (2) the length of axons and their collaterals, and (3) the entire dendritic and axonal fields produced by the neuron's arborizations.

A visual analysis was also performed in which the following parameters were addressed: (1) the number of principal dendrites that emerged from the perikarya; (2) the subsequent number of branches that occurred in these principal dendrites inclusive of first, second, third and higher order segments; and (3) the number of axon collaterals that occurred.

RESULTS

These results were based upon data from 30 neurons in which the dendritic tree and proximal axon were labelled with horseradish peroxidase (HRP) reaction product. All neurons were reconstructed via camera lucida drawings which were then morphometrically analyzed as set forth in the Materials and Methods section. Data from an additional eleven neurons showed incomplete labelling of neurons and were consequently not included. Because of the difficulty associated with the impaling of cells with electrodes that can also pass HRP electrophoretically, only large multipolar cells were selected. It was assumed that these cells were neurons for the following reasons: (1) they were located in the upper stratum of the monolayer on top of the glial carpet, (2) the cell bodies were not flat and were sufficiently rounded to produce a phase brightness, (3) nuclei and nucleoli were clearly visible, and (4) dendrites were tapered and branched at acute angles. It has been determined that these criteria are sufficient to select neurons in 85% of the cases (Lucas et al, 1986). This number is probably an underestimate, since it was based on spontaneous activity and no attempts were made to artificially depolarize the cell. Axons are difficult to

see with phase contrast microscopy so that axonal criteria (constant diameter and right angle collateral branching) were not used for the selection of cells.

Based on the camera lucida drawings of the labelled cells it can be concluded that the spine-free somata were oval or pyramidal in shape and ranged from 97 to 1,183 μm^2 in area corresponding to somal diameters of 11 to 35 μm. Three to seven primary dendrites arose from cell bodies and branched into third, fourth and fifth order segments to form dendritic fields whose areas ranged from 74,684 μm^2 to 557,596 μm^2. Cells with three, four, or five primary dendrites occurred most frequently, while only 7 neurons consisted of six or seven primary dendrites. None of the labelled cells had fewer than three or greater than seven primary dendrites. The total number of all dendritic branches for a given cell ranged from 10 to 46. The total dendritic length ranged from 1,435 to 5,273 μm and was calculated by summing the length of all dendritic segments. While most dendrites branched in a simple dichotomous fashion, in some cells three or more branches appeared to emerge from one point (Fig. 2). Dendrites displayed a somewhat rough contour which is a normal feature of dendrites *in situ* and arises from the numerous spines on the dendritic surface. Spines are generally thought to represent functional synapses. It is reassuring to note that these common structures are also seen in monolayer

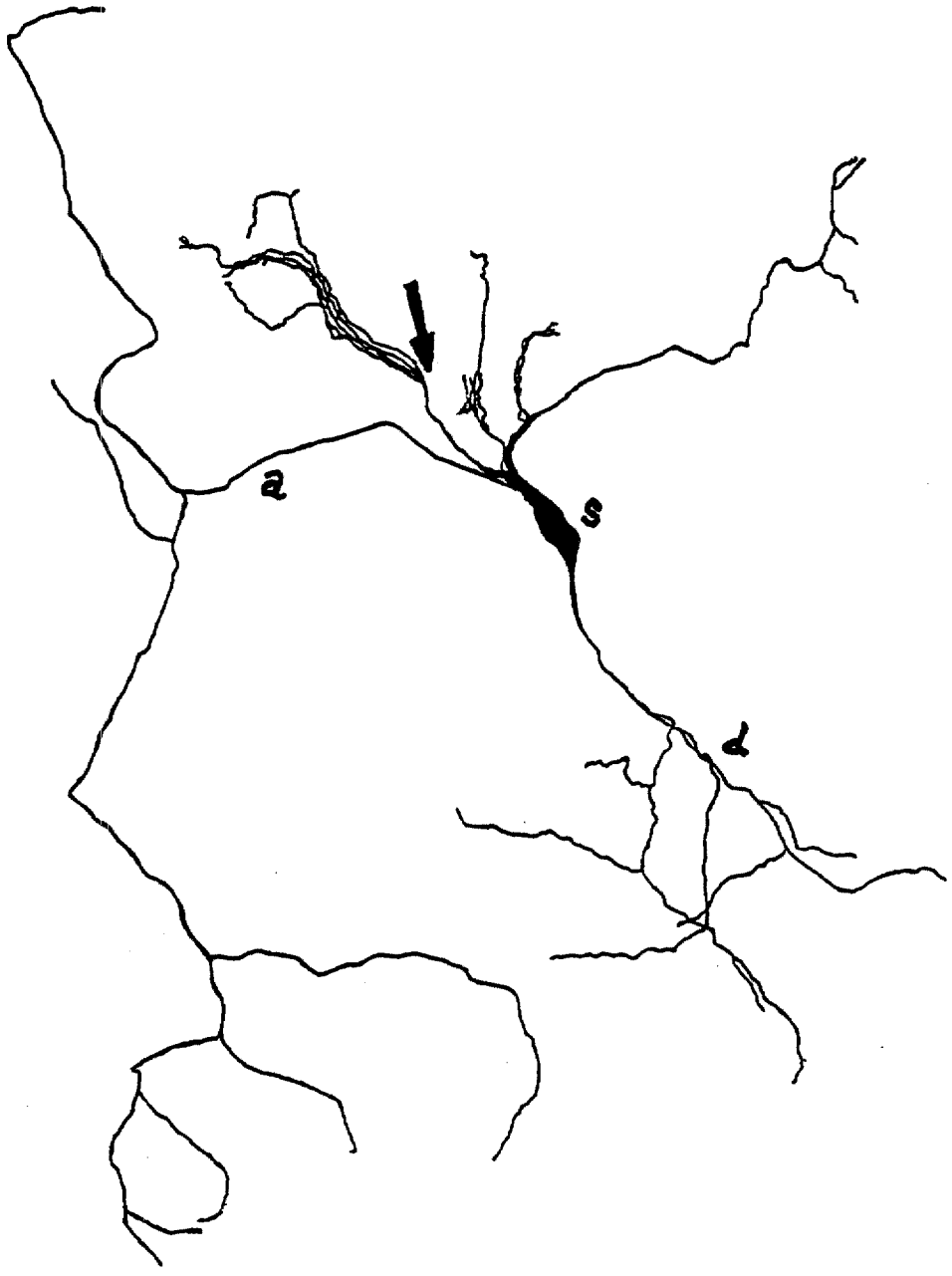

Figure 2. Reconstruction of a typical oval shaped neuron. Arrow points to a dendritic branch point in which three segments appear to emerge. Abbreviations are used to show the three main parts of the neuron. *s* (soma), *d* (dendrites), and *a* (axon).

cultures. This represents further support for the general assumption that the common synaptic mechanisms and structures are preserved. A high magnification light microscopic photograph of spine and bouton structures is shown in Fig. 3.

Of 30 neurons, 27 had identifiable axons as determined by clear axon hillock, nontapering contours, and right angle collaterals. However, the axons were assumed to be filled in only 21 of these 30 labelled neurons. The remaining 9 axonal segments were thought to be incompletely labelled because they were shorter than the dendritic tree. Total labelled axon length ranged from 615 to 2,299 μm. Some axons did not branch while others produced as many as seven primary and secondary bifurcations. Axonal fields ranged from 32,979 to 946,264 μm^2. The shortness of some axons was attributed to a lack of transport resulting from severe damage to the cell.

Neurons were separated into two major categories according to their cell shape. These are pyramidal shaped neurons and oval shaped neurons. The parameters for the average neuron are summarized in Tables 1 & 2.

Figure 3. Light microscopic photographs of spine and bouton structures. Arrow points to synapse formation. Photograph B illustrates the contour differences between smooth axons on left and rough contour dendrites on right.

Table 1. Average parameters for oval shaped neurons.

PARAMETER	MEAN	n=	STD. DEV.
SOMAL DIAMETER (μm)	25.6	20	5.1
TOTAL DENDRITE LENGTH (μm)	2,973	20	1,094
DENDRITIC FIELD (μm2)	2.37×10^5	20	1.32×10^5
DENDRITE DOMAIN (μm2)	103.9	20	24.9
TOTAL DENDRITIC BRANCHES	20.6	20	8.5
DISTANCE TO 1ST DENDRITIC BRANCH (μm)	63.5	20	42.0
# PRIMARY DENDRITES	4.6	20	1.4
MEAN PRIMARY DENDRITE DIAMETER (μm)	3.9	20	1.2
MAIN AXON LENGTH (μm)	727	14	520
TOTAL AXON LENGTH (μm)	1,289	14	1,039
AXON FIELD (μm2)	3.48×10^5	14	2.07×10^5

Table 2. Average parameters for pyramidal shaped neurons.

PARAMETER	MEAN	n=	STD. DEV.
SOMAL DIAMETER (μm)	22.4	10	5.7
TOTAL DENDRITE LENGTH (μm)	3,237	10	2,430
DENDRITIC FIELD (μm2)	1.8×10^5	10	$.65 \times 10^5$
DENDRITE DOMAIN (μm2)	103.3	10	45.4
TOTAL DENDRITIC BRANCHES	25.4	10	10.9
DISTANCE TO 1ST DENDRITIC BRANCH (μm)	61.5	10	44.7
# PRIMARY DENDRITES	4.3	10	1.2
MEAN PRIMARY DENDRITE DIAMETER (μm)	3.2	10	.78
MAIN AXON LENGTH (μm)	1,134	7	615
TOTAL AXON LENGTH (μm)	2,124	7	728
AXON FIELD (μm2)	4.85×10^5	7	2.6×10^5

Analysis of Dendritic Morphology

Relationship Between Equivalent Somal Diameter and Dendritic Morphology

In the living state, somal diameters are most readily determined with phase contrast microscopy. However, detailed dendritic morphology (especially at the tips) and detailed axon morphology can not be readily determined with light microscopy. Consequently, any neuronal characteristics that can be statistically linked to the size and/or shape of the soma would be of great help to an initial network mapping in the living state. The equivalent somal diameter was determined from the area by assuming a circular symmetry. Dendritic field is described in Figure 4 and represents the maximum x and maximum y distance which surrounds all dendritic processes. Total dendritic field was plotted against equivalent somal diameter for oval (Fig. 5a) and pyramidal (Fig. 5b) cell types. The distribution of data points for both oval and pyramidal cells indicates that the dendritic field increases with increasing equivalent somal diameter. A correlation coefficient of 0.90 was calculated for pyramidal shaped neurons when the two less common, small diameter neurons were disregarded. It may be possible to interpret the scatter plot representing oval shaped neurons as two separate functions which might suggest that two cell subtypes might exist. Attempts to differentiate between

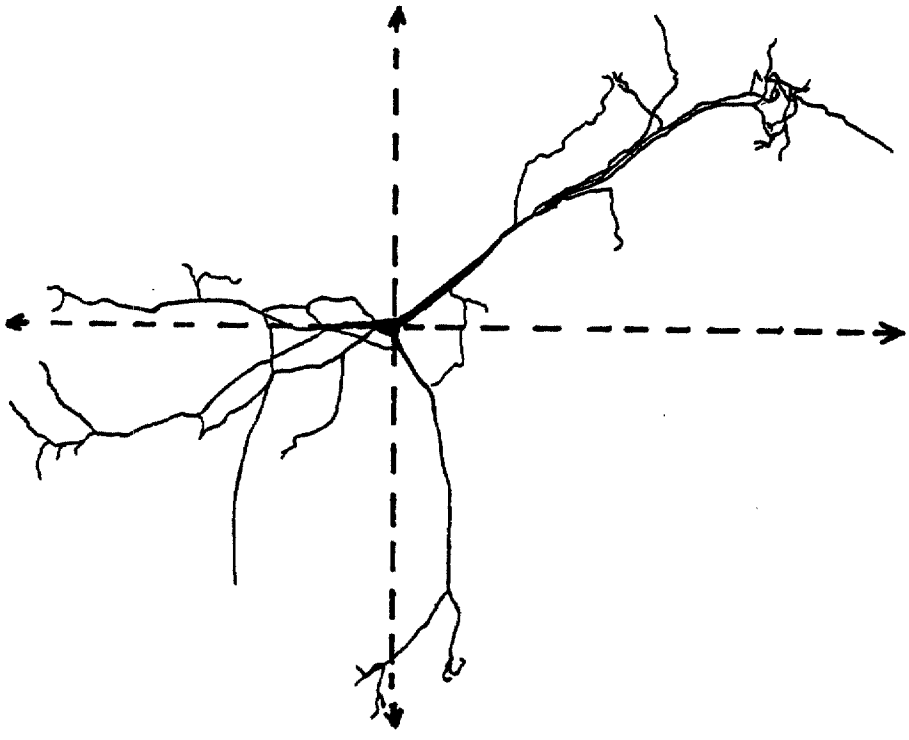

Figure 4. Reconstruction of a neuron illustrating the method of measurement for dendritic field. These lines represent the maximum *x* and maximum *y* distance surrounding all of the dendritic processes. The same method of measurement was used to determine the axonal field for neurons.

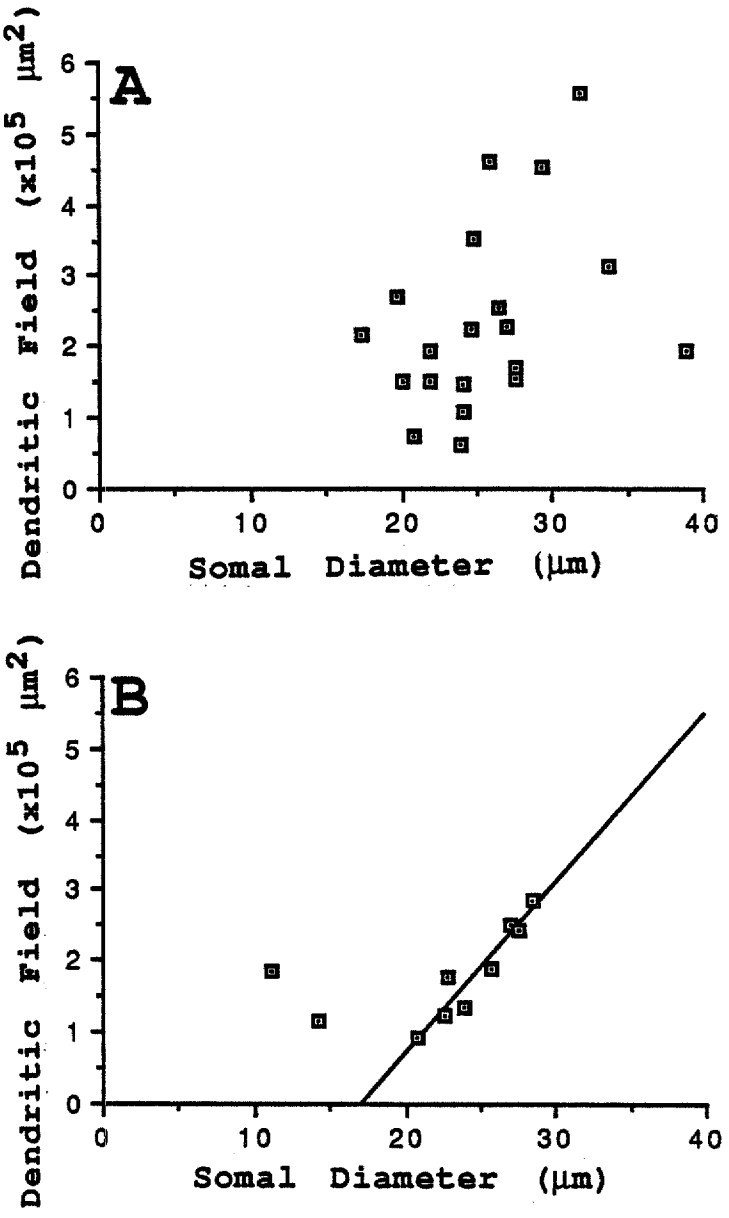

Figures 5 a & b. Diagrams illustrating the relationship between somal diameter and dendritic field. **A** represents oval shaped neurons, while **B** represents pyramidal shaped neurons. The results indicate that dendritic field increases with increasing somal diameter. A correlation coefficient of 0.90 was calculated for pyramidal shaped neurons when the two less common, smaller neurons were disregarded.

these functions was made by main axon length, total axon length, and number of primary dendrites. However, no obvious parameter could be assigned to one or the other putative function.

In order to establish a more accurate relationship between equivalent somal diameter and the domain occupied by dendrites a new parameter was established; dendrite domain. Dendrite domain was determined by closely drawing a line surrounding all of the dendritic processes while eliminating as much unoccupied space as possible (Fig. 6). Dendrite domain is more representative of the actual area covered by dendritic segments and may prove useful for future network mapping. Equivalent somal diameter was then plotted against dendrite domain for oval (Fig. 7a) and pyramidal (Fig. 7b) cell types. The graphs representing both pyramidal and oval shaped neurons show no obvious correlation between these two parameters.

The sum of the primary dendrite diameters for a given cell was plotted against equivalent somal diameter for oval (Fig. 8a) and pyramidal (Fig. 8b) cell types. Dendrite diameters were measured for each cell at the base of each primary dendrite. A relationship was shown between the sum of the primary dendritic diameters versus equivalent somal diameter for oval shaped neurons; whereas a less convincing relationship exists for pyramidal shaped neurons. The distribution of data points indicates that the sum of

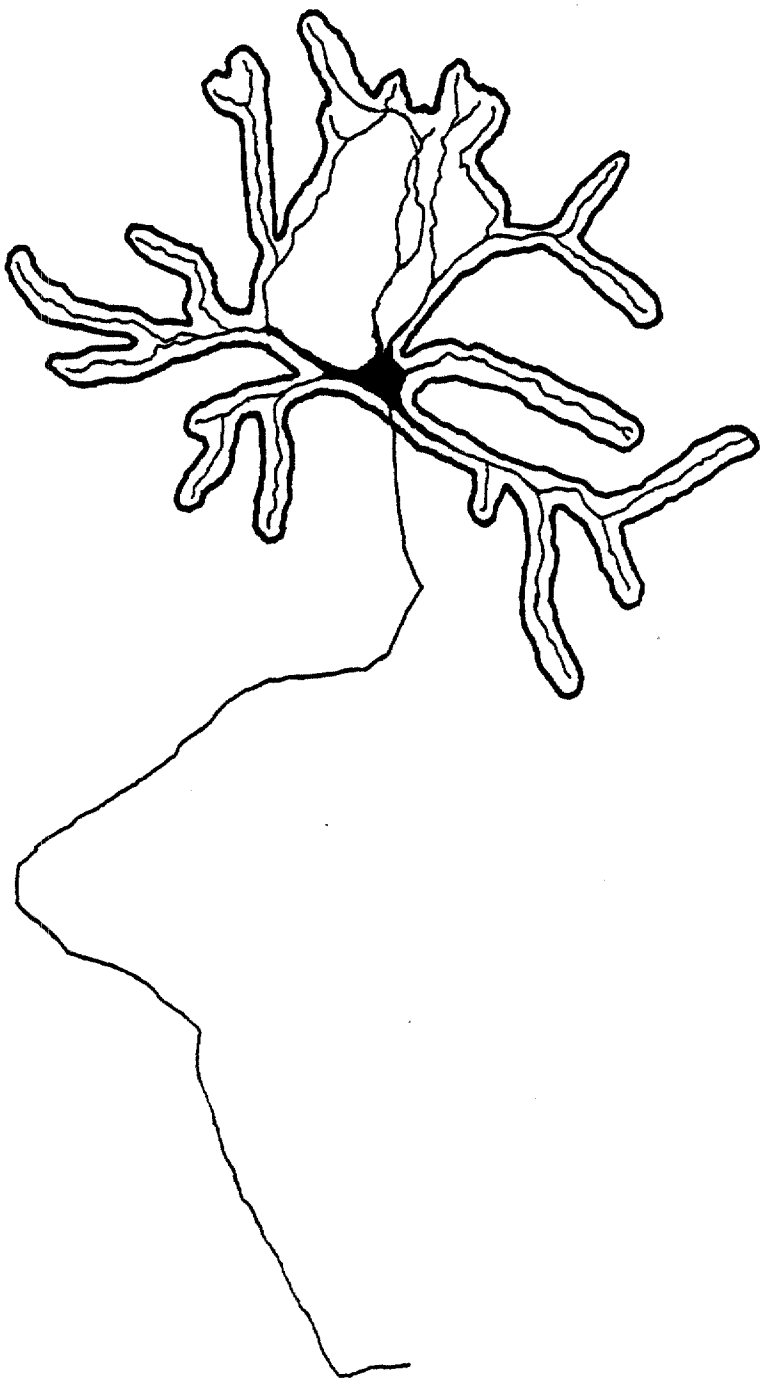

Figure 6. Reconstruction of a neuron illustrating the method of measurement for dendrite domain. This was determined by closely drawing a line surrounding all of the dendritic processes while eliminating as much unoccupied space as possible. This domain is more representative of the actual area covered by dendritic segments.

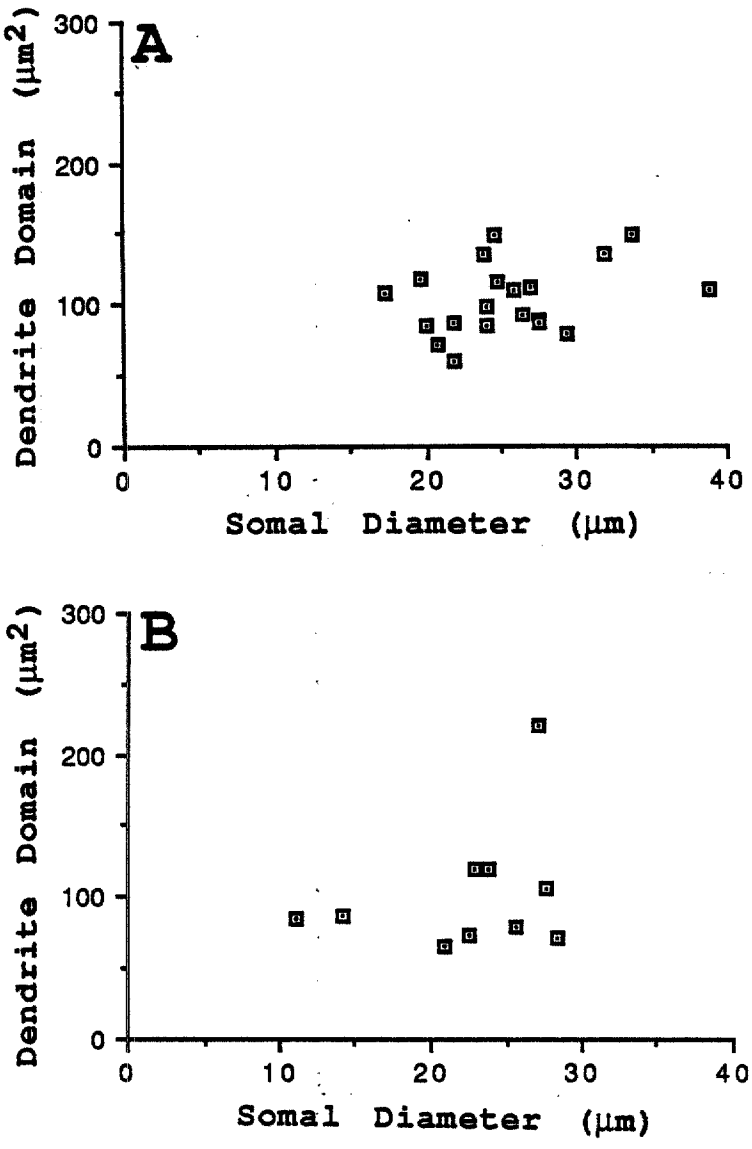

Figures 7 a & b. Diagrams illustrating the relationship between somal diameter and dendrite domain. **A** represents oval shaped neurons, while **B** represents pyramidal shaped neurons. The distribution of data points suggests that there is no true correlation for these parameters.

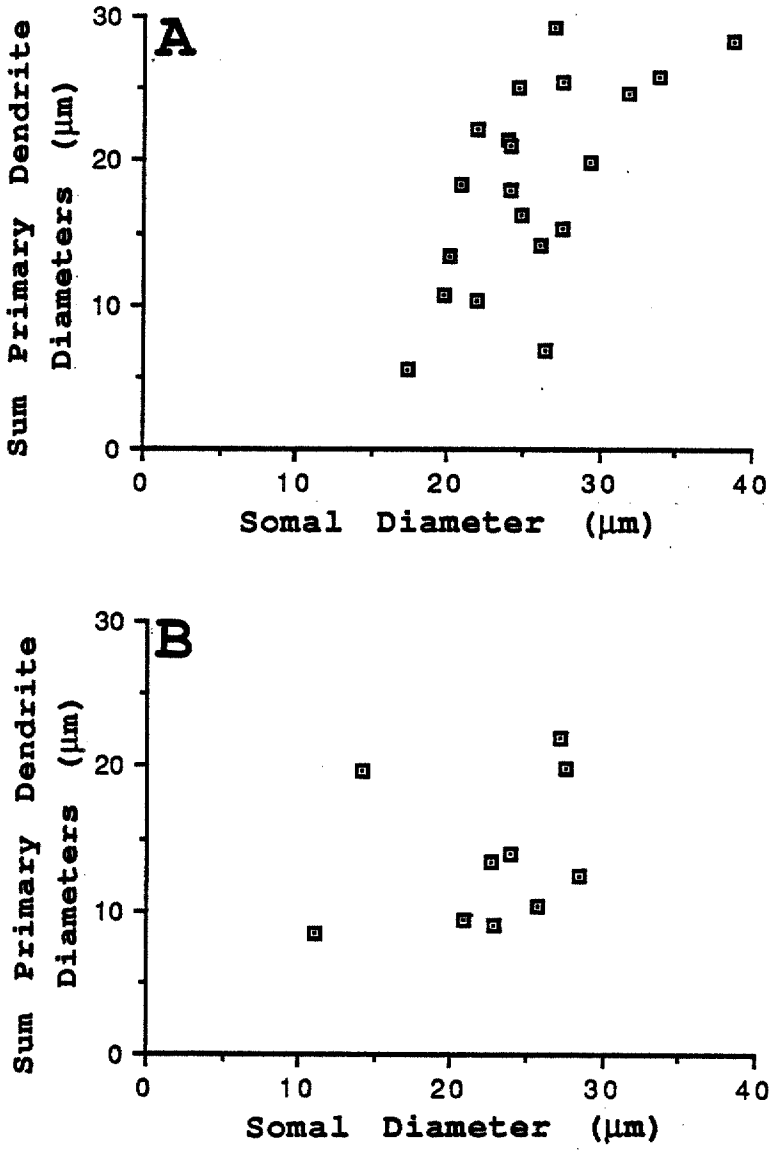

Figures 8 a & b. Diagrams illustrating the relationship between somal diameter and the sum of the primary dendrite diameters. **A** represents oval shaped neurons, while **B** represents pyramidal shaped neurons. The distribution of data points in **A** indicates that the sum of the dendritic diameter for a given cell increases relative to increasing somal diameter. A definite correlation between these two parameters can not be extrapolated for pyramidal shaped neurons.

dendritic diameters for a given cell increases relative to increasing equivalent somal diameter.

Relationship Between Primary Dendrite Diameters and Dendrite Morphology

The relationship between individual primary dendrite diameters and total dendrite length was compared in Fig. 9. The results from this graph are encouraging and demonstrate that total dendrite length increases linearly with increasing primary dendrite diameter. This relationship makes it possible for a researcher to predict the total dendrite length produced by a single primary dendrite of a given diameter and approximate the total surface area on which incoming information may be processed. The results show that total dendrite length increases an average of 125 μm per 1 μm increase in primary dendrite diameter. A correlation coefficient of 0.77 was calculated for these two parameters.

Primary dendrite diameter was plotted against dendrite domain in Fig. 10. Dendrite domain was determined by drawing a line closely around the dendritic tree resulting from each primary dendrite. The results show a convincing relationship between these two parameters indicating that individual dendrite domains increase relative to increasing primary dendrite diameters.

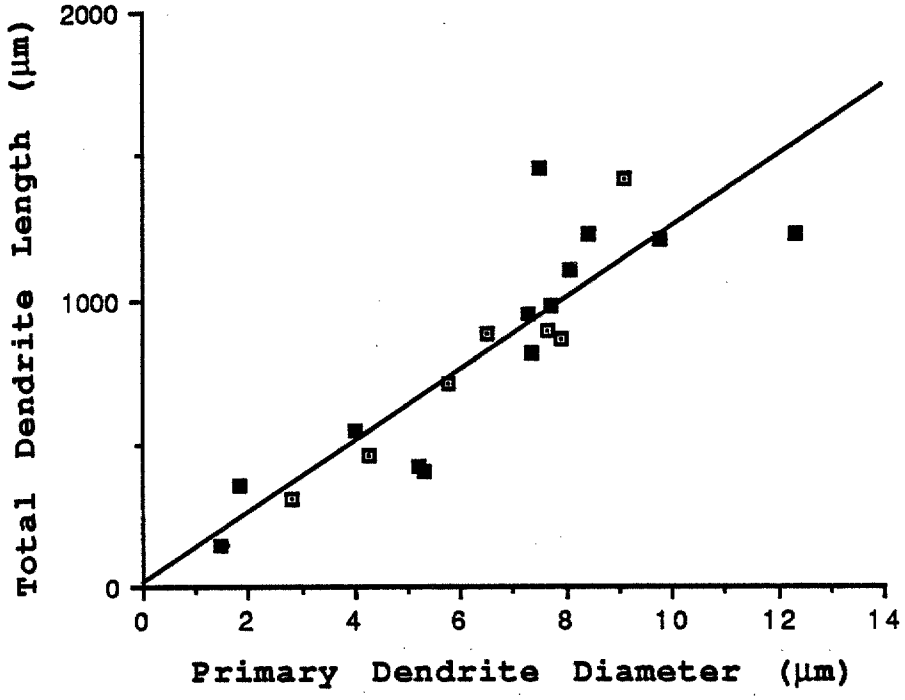

Figure 9. Diagram illustrating the relationship between primary dendrite diameter and the total dendrite length. The graph represents both oval (darkened squares) and pyramidal shaped neurons (open squares). The results show that total dendrite length increases an average of 125 µm per 1 µm increase in primary dendrite diameter. A correlation coefficient of 0.77 was calculated for these two parameters.

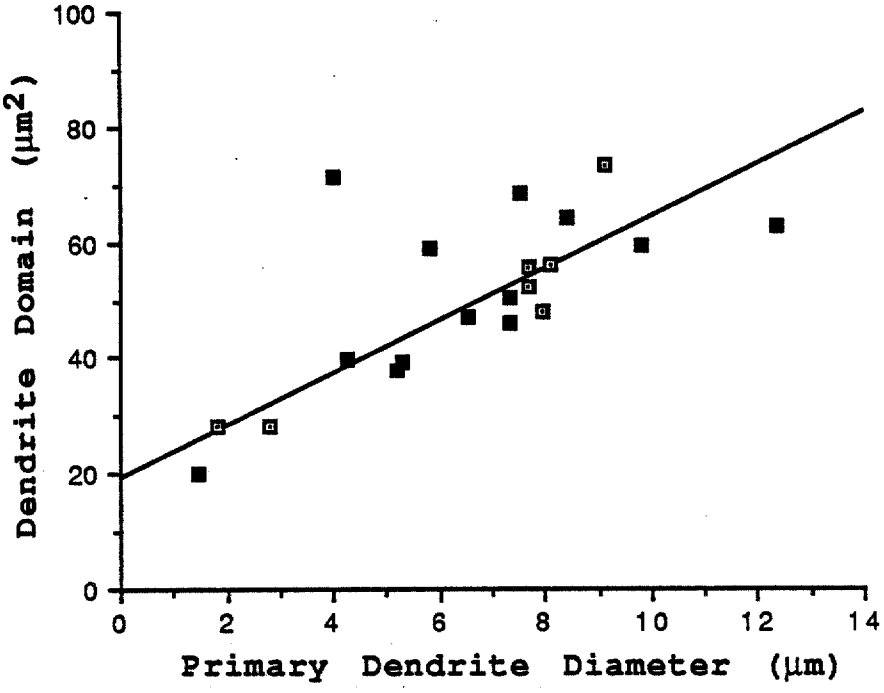

Figure 10. Diagram illustrating the relationship between primary dendrite diameter and dendrite domain. The graph represents both oval (darkened squares) and pyramidal shaped neurons (open squares). The results show a linear relationship between these two parameters indicating that dendrite domain increases with increasing primary dendrite diameter. A correlation coefficient of 0.74 was calculated for these two parameters.

A correlation coefficient of 0.74 was calculated for these two parameters.

Primary dendrite diameter was also plotted against the distance to the first dendritic branch point on a primary dendrite (Fig. 11). Two functions seem to emerge in the distribution of data points. These results suggest that the distance to the first dendritic branch point may increase relative to increasing primary dendrite diameter. The higher function exists exclusively of oval neurons while the lower function is a combination of both oval and pyramidal cell shapes.

Primary dendrite diameter was also plotted against the total dendritic branches per cell (Fig. 12). The distribution of data points suggests that the total dendritic branches increases with increasing primary dendrite diameter. The correlation coefficient calculated for this relationship is low and is the result of the broad distribution of data points.

Dendrite Length and Diameter Distributions as a Function of Distance From The Soma

In this section the percent dendrite length located in 40μm annuli was evaluated as a function of radial distance from the somata. Concentric circles, 20μm in diameter, were drawn to aid in the interpretation of the results (Fig. 13). The significance of these data stems from the assumption

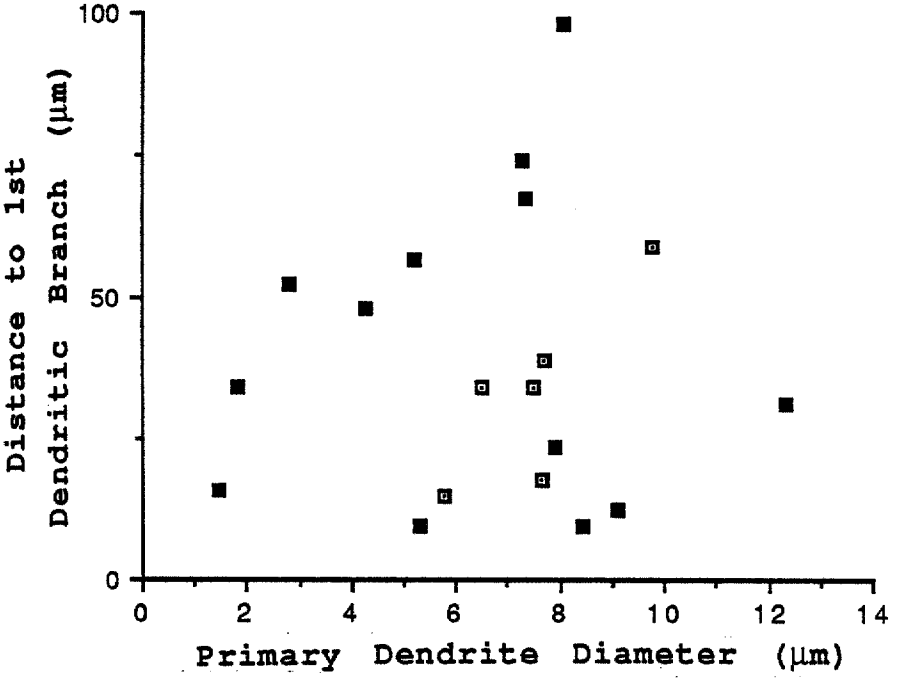

Figure 11. Diagram illustrating the relationship between primary dendrite diameter and the distance to the first dendritic branch. The graph represents both oval (darkened squares) and pyramidal shaped neurons (open squares). The results suggest that the distance to the first dendritic branch point may increase with increasing primary dendrite diameter.

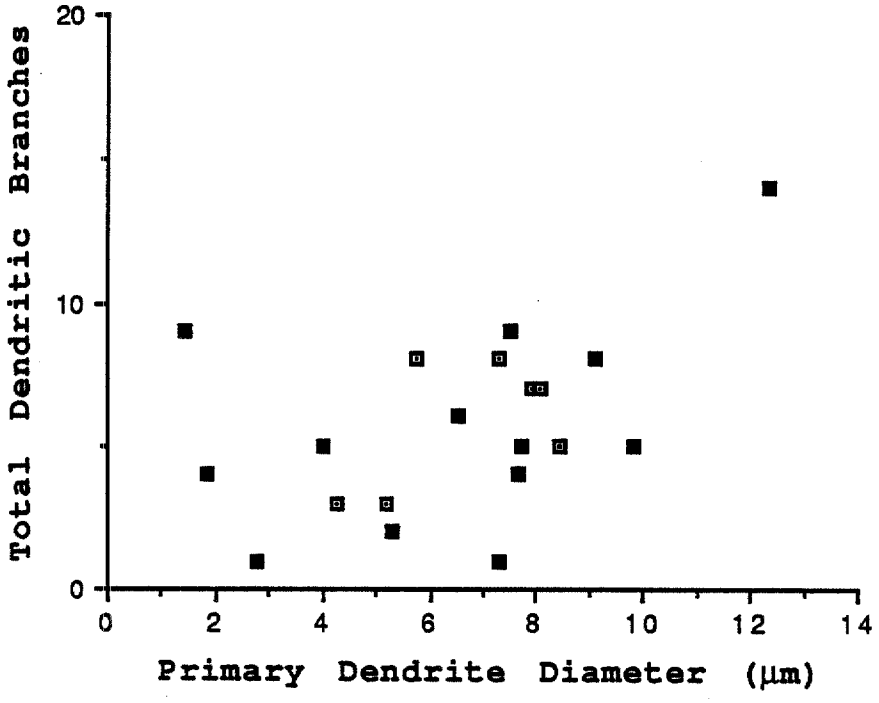

Figure 12. Diagram illustrating the relationship between primary dendrite diameter and the total dendritic branches per primary dendrite. The graph represents both oval (darkened squares) and pyramidal shaped neurons (open squares). The distribution of data points suggests that the total dendritic branches increases with increasing primary dendrite diameter. The correlation coefficient is low for this relationship.

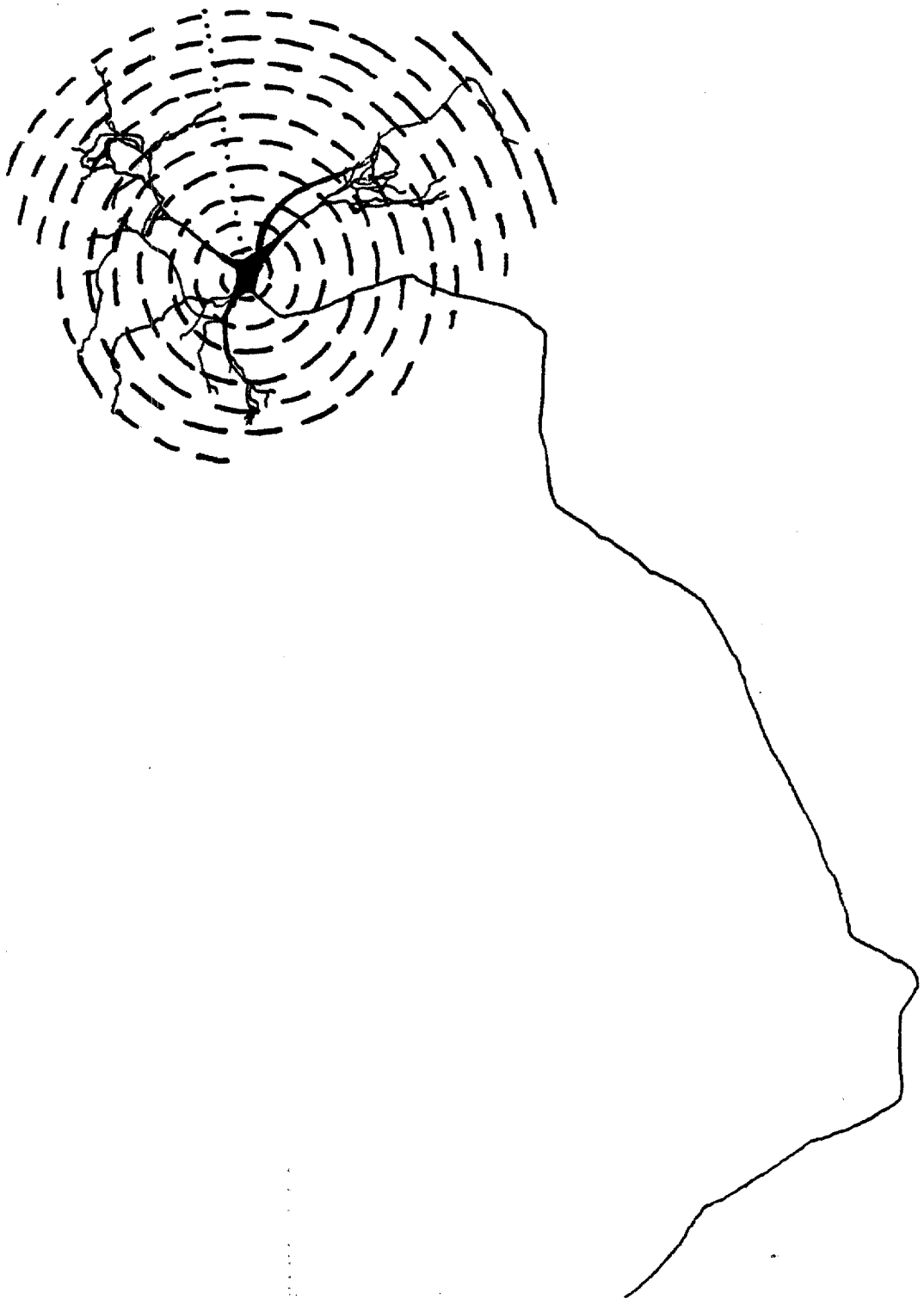

Figure 13. Reconstruction illustrating the method of measurement of percentage of dendrite length as a function of radial distance from the cell soma. Annuli are 20μm in diameter each. Measurements were made in 40μm segments.

that a greater dendrite length would produce a greater dendrite surface area on which synaptogenesis might occur. If synaptogenesis is found to be relatively constant per dendrite length (or surface area), then the location of the greatest dendrite mass would also represent the location of the largest number of synaptic inputs. Histograms representing one oval and one pyramidal shaped neuron are shown in figures 14 a & b. A bell shaped curve was observed for most of the cells investigated. Figures 15 a & b represent a sample of five oval and five pyramidal shaped neurons respectively. The data indicate that the greatest percentage of total dendrite length existed approximately 120-200μm from the cell soma. As expected, the smallest percentage of total dendrite length existed nearest to the cell and at distances greater than 300μm from the cell body. Cumulatively, there existed a strong tendency for the percent total dendrite length to increase with distance from the cell soma to a certain point at which a maximum was achieved followed by a decrease in the percent total dendrite length to the terminal segments.

Mean dendrite diameter was plotted against the distance from the cell soma to determine the rate of taper along the dendrite (Fig. 16). Five measurements were taken per ten μm distance along the course of a primary dendrite to its termination. The results show that the dendrite decreased in diameter with distance from the soma with a

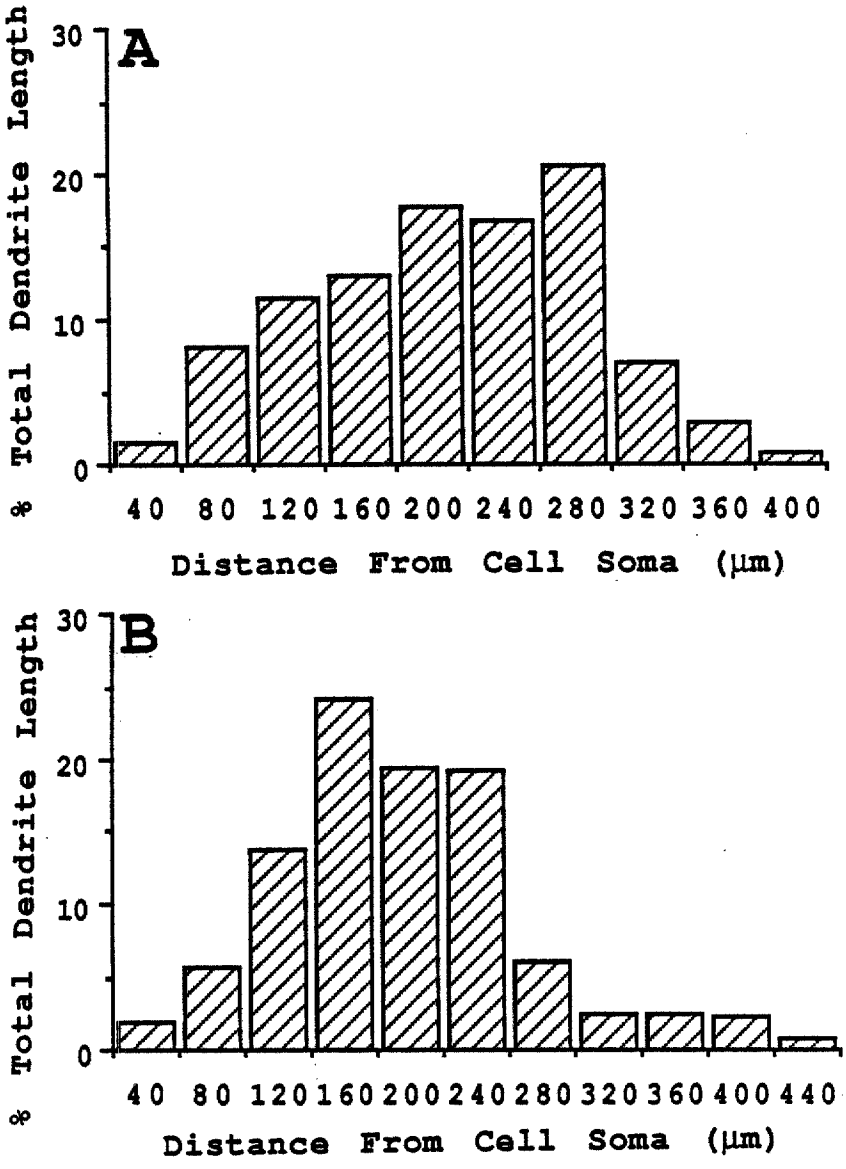

Figures 14 a & b. Histograms illustrating the percent total dendrite length located in 40 µm annuli as a function of radial distance from the soma. **A** represents one oval shaped neuron and **B** represents one pyramidal shaped neuron. The results demonstrated that the smallest percentage of dendrite length existed nearest to the cell soma and at distances greater than 300 µm from the cell body.

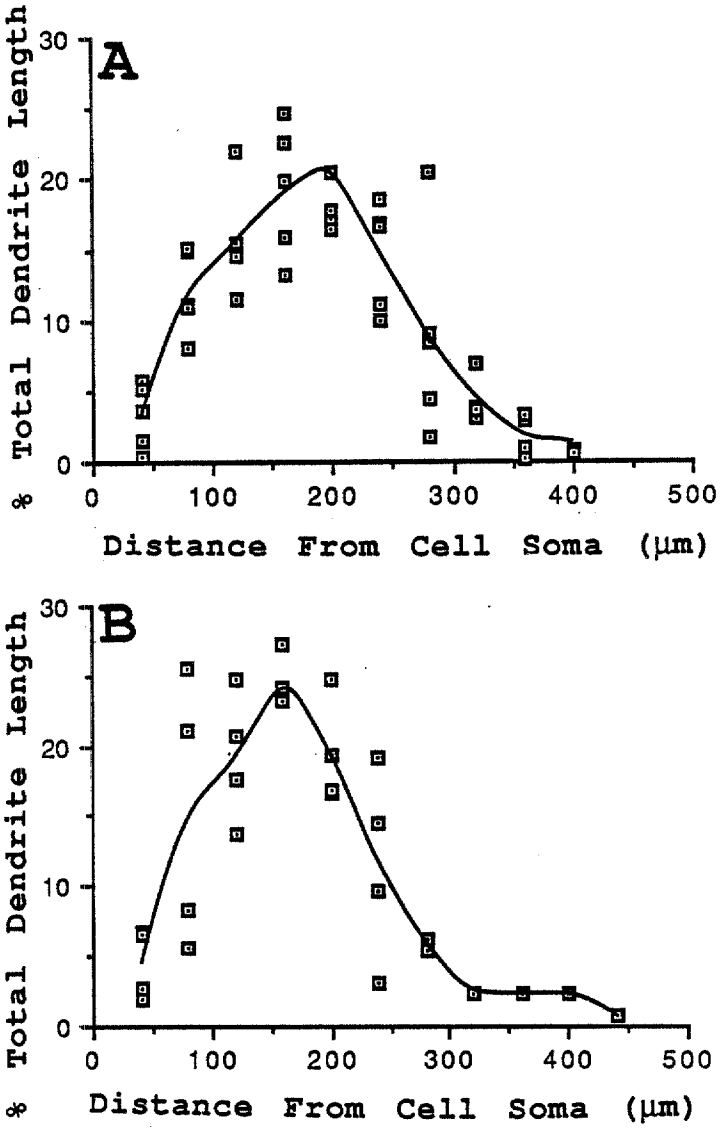

Figures 15 a & b. Diagrams illustrating the relationship between distance from the cell soma and percent total dendrite length. **A** represents a sample of 5 oval shaped neurons while **B** represents a sample of 5 pyramidal shaped neurons. The results indicate that the greatest percentage of total dendrite length existed approximately 120-200 µm from the cell soma. The curve derived is a function representing a 3rd order polynomial.

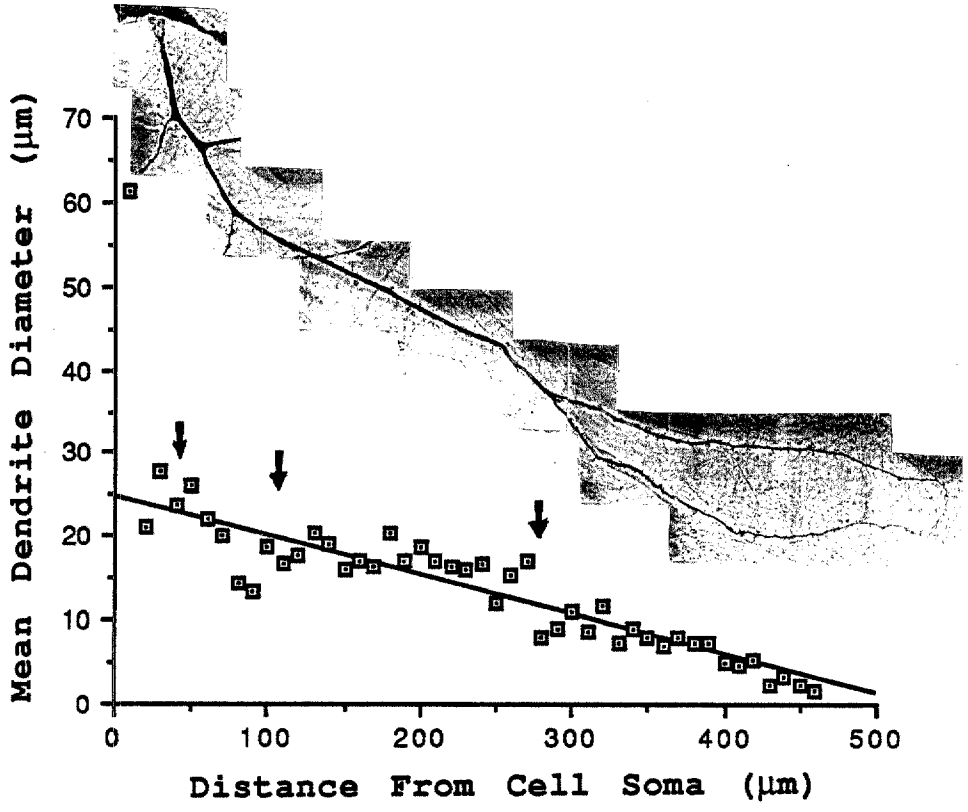

Figure 16. Diagram illustrating the relationship between distance from the cell soma and mean dendrite diameter. The points represent the mean of five measurements taken per 10 µm distance along the course of a primary dendrite to its termination. Arrows point to distances at which branch points occurred. The results show that the dendrite decreased in diameter with distance from the soma with a taper ratio of 6 µm diameter per 100 µm distance. A correlation coefficient of .86 was calculated when the first diameter measurement was disregarded. Photographs showing the dendrite under investigation are also shown.

taper ratio of 6 μm diameter per 100 μm distance. A correlation coefficient of 0.86 was calculated for this relationship. A photograph of the taper investigated is also shown. Some important observations from this analysis are that a rapid taper occurs at the base of the primary dendrite to the first dendritic branch point, the tapering of the dendrite along the midsection of the dendrite is minimal and almost absent, and that the most continuous taper occurs at the terminal segment (after the last branch point) to the termination of the dendrite.

Attempts were made to verify the concept that dendrites in culture follow the 3/2 rule as proposed by Rall in 1962. The rationale for the 3/2 rule is that there is a great need for making simplified equivalent neurons to model the morphological complexity. The 3/2 rule proposes that the diameter of a parent dendrite segment taken to the 3/2 will be equal to the sum of the daughter segment diameter taken to the 3/2. According to Horwitz (1981), the monolayer network would eventually be modeled as a collection of interconnected simplified neuronal structures. Figure 17 illustrates the manner in which measurements were taken from the dendrites and includes the formula which is used for the 3/2 rule. Table 3 lists the 15 measurements that were taken and the observed and expected 3/2 diameters with the percent deviation for each. A measurement error of 6% was calculated after taking 20 measurements at a

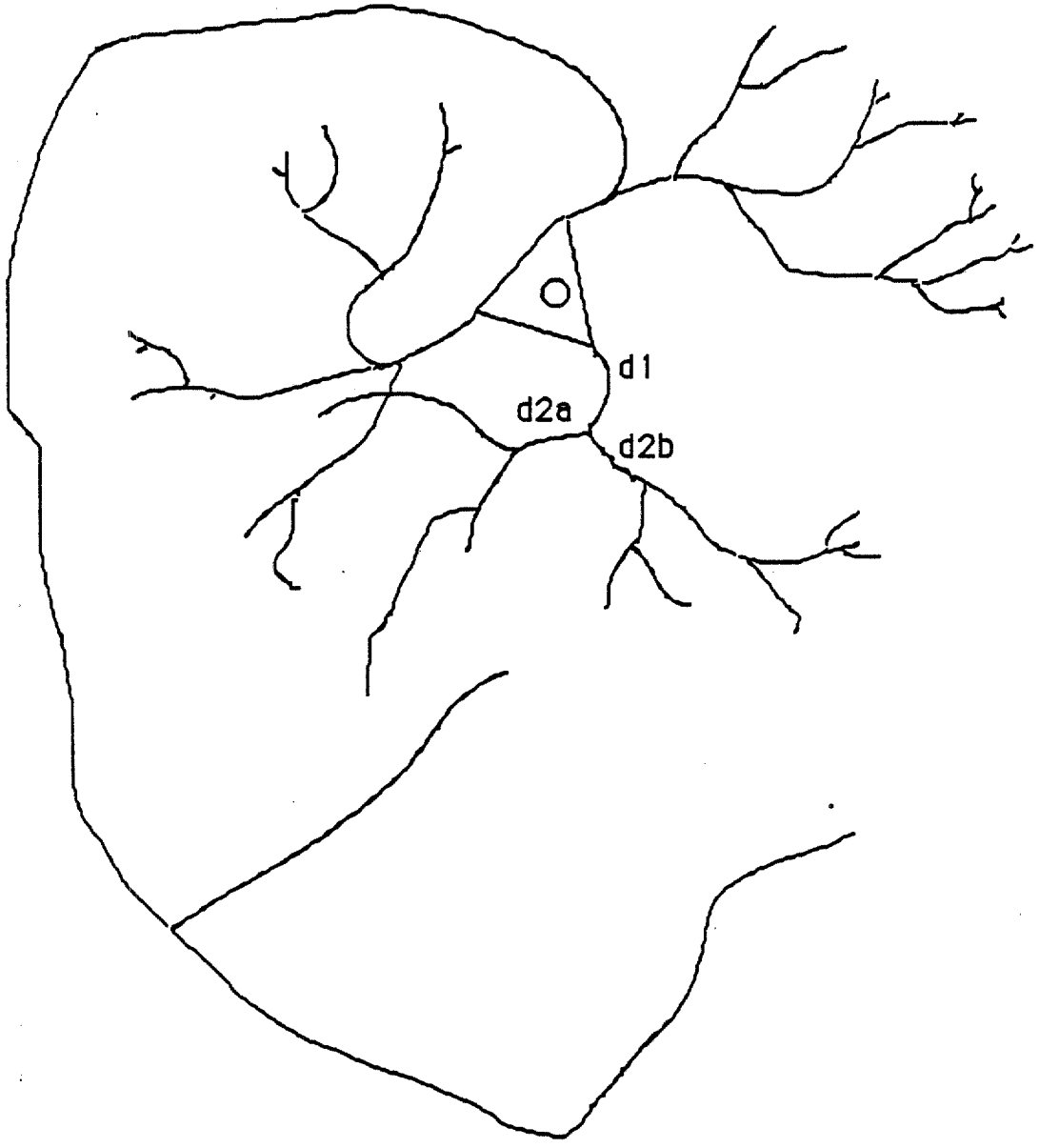

$$d1^{3/2} = d2a^{3/2} + d2b^{3/2}$$

Figure 17. Computer drawing illustrating the points of measurement for calculating the 3/2 rule as proposed by Rall and the formula used for the results.

Table 3. Table of measurements used for 3/2 rule data.

Msmt	d2a	d2b	d1 Actual	d1 Expected	% Deviation
1	1.61	0.91	2.19	2.52	-13.10
2	2.82	1.19	1.61	4.01	-59.85
3	0.65	1.09	2.82	1.74	+52.87
4	2.07	1	2.32	3.07	-24.43
5	0.82	1.39	2.07	2.21	-6.33
6	1.61	2.32	3.38	3.93	-13.99
7	1	1.09	2.32	2.09	+11.00
8	1	0.73	1	1.73	-42.20
9	1.09	3.52	5.99	4.61	+29.93
10	1.09	2.83	3.52	3.92	-10.20
11	2.83	1.61	4.72	4.44	+6.31
12	1.61	1.84	3.8	3.45	+10.14
13	3.8	1.61	4.1	5.41	-20.52
14	2.32	0.65	2.69	2.97	-9.43
15	1.61	0.73	2.32	2.34	-.85

20 diameter measurements used to calculate error

Msmt	in µm	Msmt	in µm
1	1.94	11	1.81
2	1.94	12	1.88
3	1.69	13	1.88
4	1.81	14	1.97
5	1.88	15	1.66
6	1.75	16	1.81
7	1.69	17	1.88
8	1.75	18	1.88
9	1.88	19	1.88
10	1.56	20	1.81

Mean = 1.82
Standard Deviation = .11
% Deviation = 6.04%

specified branch point of a single dendrite and is tabulated along with Table 3. The percent deviation in culture exceeds the measurement error in 12 out of the 15 measurement points. These results indicate that the 3/2 rule does not apply to these cultures. Other researchers have made similar attempts to confirm the validity of the relationship for motorneurons and have shown similar substantial deviations from the 3/2 rule.

Miscellaneous Relationships Between Dendrite Parameters

Dendrite domain was plotted against total dendrite length for oval (Fig. 18a) and pyramidal (Fig. 18b) cell types. The results indicate a strong correlation between these two parameters suggesting that the dendrite domain increases with increasing total dendrite length. A correlation coefficient of 0.88 was calculated for the relationship which exists for oval neurons while the correlation coefficient for pyramidal shaped neurons was 0.92.

Total dendrite length was compared to total number of dendritic branches per cell for oval (Fig. 19a) and pyramidal (Fig. 19b) cell types. The distribution of data points for both oval and pyramidal neurons indicates that total dendrite length generally increases with increasing dendritic branches per cell.

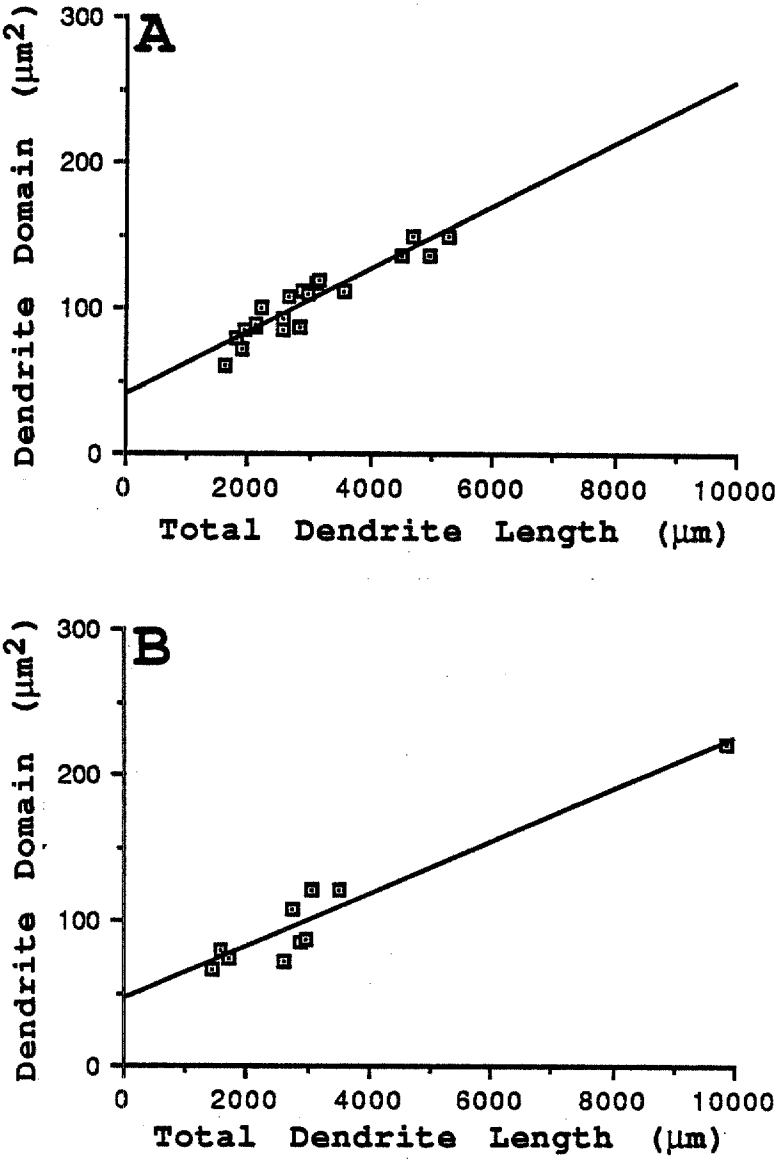

Figures 18 a & b. Diagrams illustrating the relationship between total dendrite length and dendritic domain. **A** represents oval shaped neurons, while **B** represents pyramidal shaped neurons. The results indicate a strong correlation between these two parameters suggesting that dendritic domain increases with increasing total dendrite length. A correlation coefficient of 0.88 was calculated for the relationship which exists for oval neurons while the correlation coefficient for pyramidal shaped neurons was 0.92.

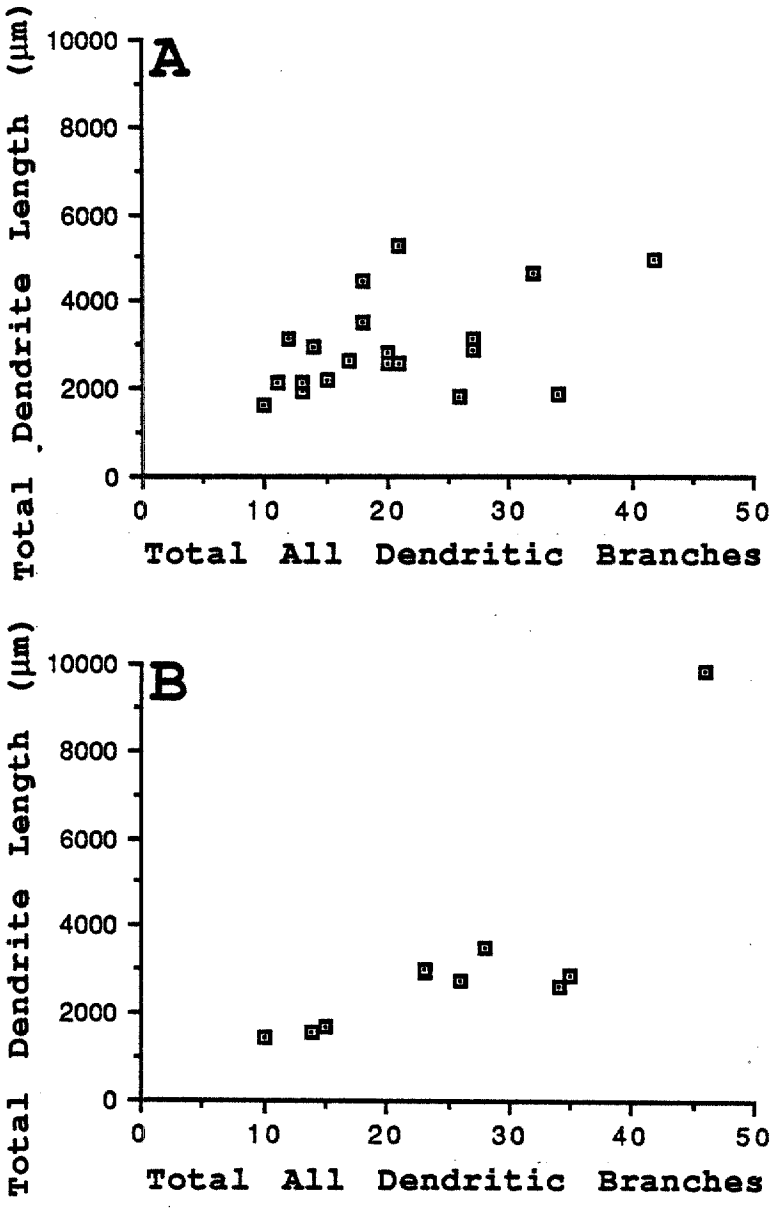

Figures 19 a & b. Diagrams illustrating the relationship between the total of all dendritic branches and total dendrite length. **A** represents oval shaped neurons, while **B** represents pyramidal shaped neurons. The distribution of data points indicates that total dendrite length generally increases with increasing dendritic branches per cell. The correlation coefficient for pyramidal shaped neurons was calculated to be 0.63.

Additionally, dendritic field was shown to increase with increasing total dendritic branches per cell for oval (Fig. 20a) and pyramidal (Fig. 20b) cell types. Pyramidal neurons showed the most convincing linear relationship between these parameters. This correlation indicates that a greater number of dendritic branches per cell influences the size of the dendritic field produced. The slope in Fig. 20b indicates that dendritic field increases an average of 7.5 x 10^4 μm^2 per 10 dendritic branches.

Analysis of Axonal Morphology

Classification of Axonal Morphology As A Function of Equivalent Somal Diameter

As mentioned previously, it was hypothesized that somal diameter might be used in electrophysiological experiments to estimate the axonal and dendritic domains produced by these cells. Consequently main axon length was plotted against equivalent somal diameter to determine if a relationship existed between these two parameters. Oval and pyramidal shaped neurons both demonstrated that main axon length generally increases with increasing equivalent somal diameter (Fig.'s 21 a & b). Cells whose axon could not be identified or which exhibited obvious incomplete filling were not included in these data.

Equivalent somal diameter was then plotted against total axon length (main axon length plus collaterals) for

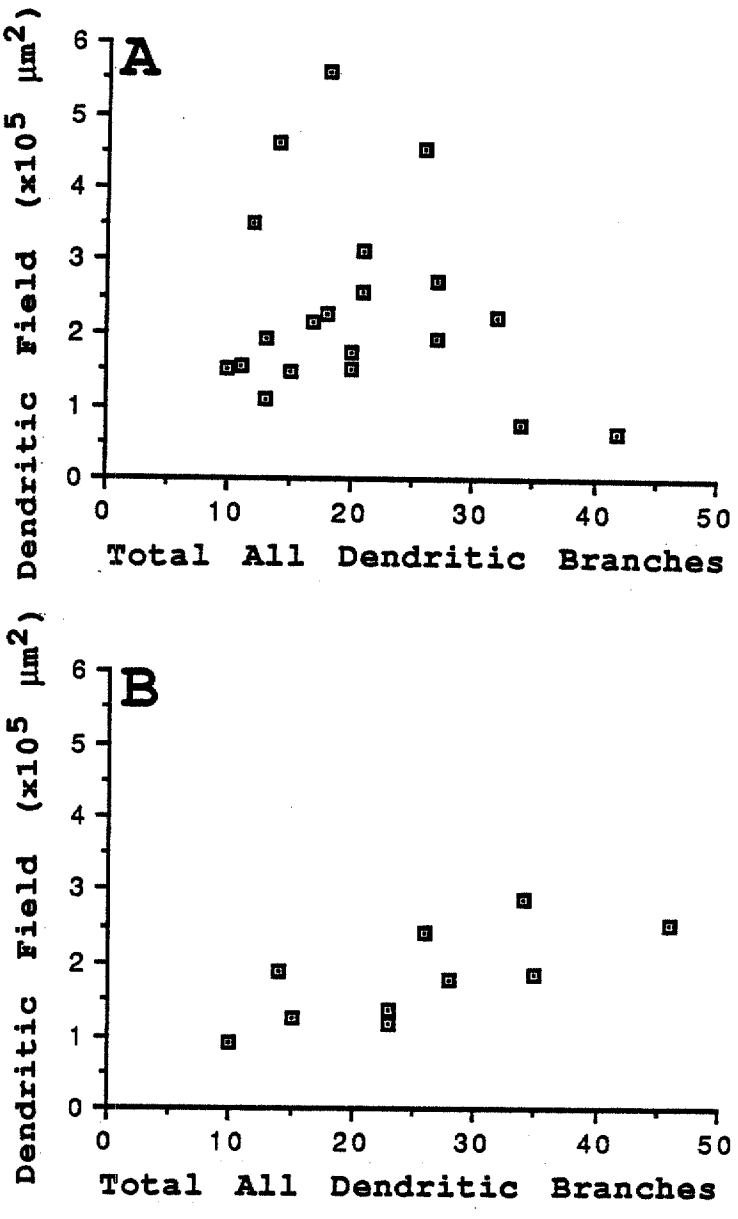

Figures 20 a & b. Diagrams illustrating the relationship between total dendritic branches per cell and dendritic field. **A** represents oval shaped neurons, while **B** represents pyramidal shaped neurons. The distribution of data points indicates that dendritic field increases with increasing number of dendritic branches. The slope in figure 20 b indicates that dendritic field increases an average of 7.5×10^4 μm^2 per 10 dendritic branches.

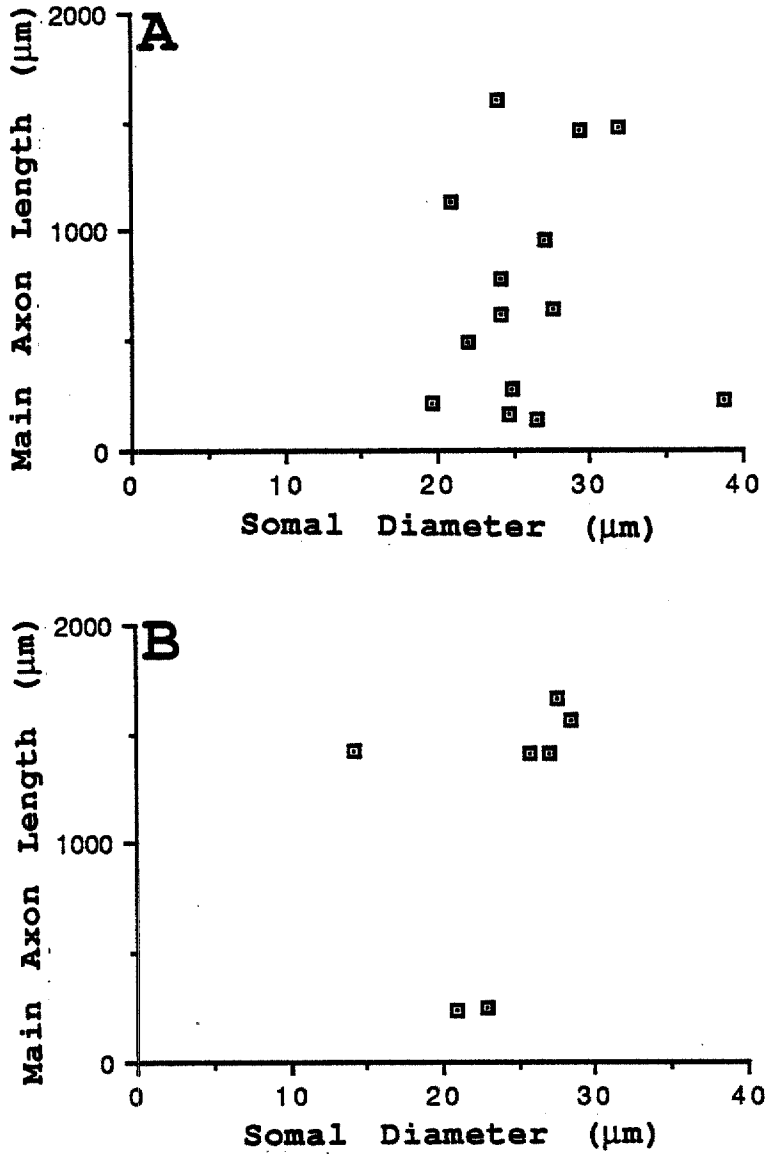

Figures 21 a & b. Diagrams illustrating the relationship between somal diameter and main axon length. **A** represents oval shaped neurons, while **B** represents pyramidal shaped neurons. Distribution of data points suggest that main axon length generally increases with increasing somal diameter.

oval (Fig. 22a) and pyramidal (Figs. 22b) cell types. Distribution of data points indicates that total axon length may increase with increasing equivalent somal diameter. However, it is important to elaborate that had 100% completeness of labelling been achieved a more definable and convincing correlation between these parameters may have resulted.

Neurons Without Axons

A crucial question for network electrophysiology is the presence of cells without axons which are thought to process information on the subthreshold level and produce no action potentials. Such cells would not be detected by extra-cellular recording techniques and would therefore represent silent neurons in the network. Regions of the central nervous system which have a high percentage of silent neurons would not be of optimal use for the multimicroelectrode techniques used in this laboratory. Therefore, it is an important part of this project to ascertain the percentage of neurons in which axons could not be identified.

Three of the 30 analyzed cells displayed no clearly identifiable axon. These cells were scrutinized with a new Zeiss Axiophot microscope at a magnification of 1200x. The criteria mentioned in the methods section were applied to distinguish between axons and dendrites. It was assumed

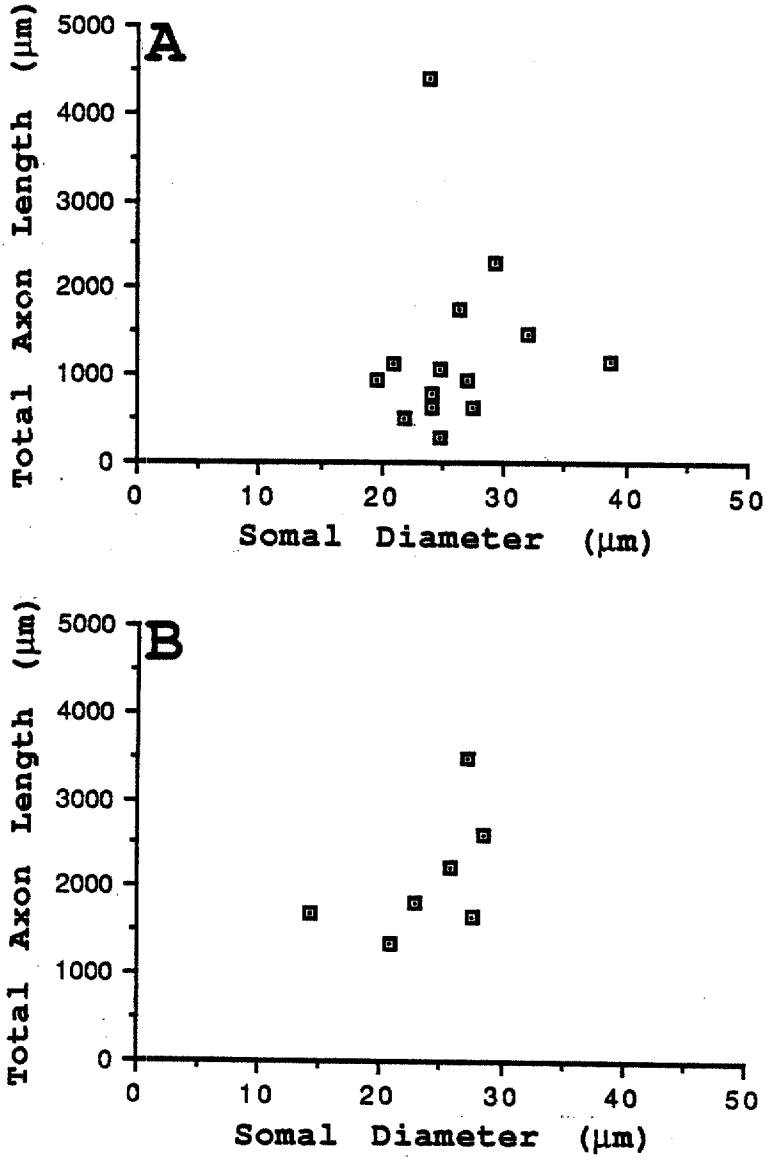

Figures 22 a & b. Diagrams illustrating the relationship between somal diameter and total axon length. **A** represents oval shaped neurons, while **B** represents pyramidal shaped neurons. Distribution of data points suggests that total axon length may increase with increasing somal diameter.

that if the dendritic tree was essentially completely filled then a short segment of the axon must also be stained. As a result those cells with no visible axons must either be Golgi Type II cells or are misidentified noneuronal cells.

DISCUSSION

Highlights

The ability to identify any parameter, observable with light microscopy, that could be used to predict other cell features not visible in cell culture was a major goal of this project. This has, to a good extent, been achieved. From the database established in this study, it is now possible to generate certain predicted values for the portion of a neurons dendritic domain that is not visible in culture. A linear relationship was established between primary dendrite diameter and total dendrite length (Fig. 9). The significance of this finding is that the researcher can approximate the total surface area on which incoming information may be processed for a given neuron in culture. In addition, a linear relationship was demonstrated for primary dendrite diameter and dendritic domain (Fig. 10). Knowledge of this relationship is useful because of the complexity of dendritic branching in such cultures which makes the assessment of a single dendrite's domain very difficult.

Another result of this study deals with the percent dendrite length evaluated as a function of radial distance from the somata. The significance of these data stems from

the assumption that a greater dendrite length would produce a greater surface area over which synaptogenesis might occur. These data now allow an experimenter to predict the location of the greatest percentage dendrite length for a typical neuron.

An extrapolation of the data revealed several additional relationships. These findings may also provide useful information about the cell once more data becomes available.

It is conceivable that computer programs will be written in the future that will allow an experimenter to make predictions about cells in culture. The setup would include an image processor showing phase contrast images. A light pen could be used to measure somal and primary dendrite diameters. Those measurements alone could be used to generate the additional information needed about the neuron.

Shortcomings

It was not possible to be certain that dendrite and axon length measurements represented segments that were completely filled. Consequently, all lengths mentioned in the text and in graphs represented only "labelled lengths". The scatters may reflect the varia-bility in the percent of the segment (dendrite or axon) that was successfully labelled. This may, more specifically, account for the

separation of functions which emerged on some graphs which were proposed to be two possible cell subtypes.

Although it is generally accepted that different substrates affect the overall morphology of nerve cells, quantitative data is difficult to find in the literature. In this particular study, dissociated cells from mouse spinal cord were seeded onto glass coverslips prepared with polylysine and laminin. Furthermore, a confluent glial carpet was allowed to develop before glial growth was inhibited with FDU (Gross and Lucas 1982). The results obtained in this study must therefore be taken as valid for these specific conditions. Other studies will be required on different substrates to demonstrate that these graphs have a more general significance.

A second shortcoming of this study was the limited size of neurons impaled and the age of the cultures used. For the most part, large multipolar cells were selected for injection purposes as opposed to the smaller bipolar cells which are characteristically difficult to impale and hold. In addition, all of the cells selected were 4 to 6 weeks of age. Therefore, only a limited sample of neurons is represented and future experiments would certainly be justified. However, it should be mentioned that good cultures with very large cells are not always available and that these types of investigations would be very time consuming.

One disappointment of the study was that these results could not be compared to networks grown on multielectrode plates. Of two experiments attempted on these plates only one neuron demonstrated the HRP reaction product. This neuron was not included as data due to an underdeveloped dendritic tree and short axon which resulted due to an inconsistency of the glial carpet. As stated earlier, the main problem encountered is the availability of good cultures with very large cells. Additional experiments with these multielectrode plates would be especially useful to this laboratory. A study of this sort could provide information for mapping cell circuitry in small monolayer cultures so that electrical activity could be correlated with network structure.

Other Findings

An important finding resulting from this study is in regard to the many unsuccessful attempts to impale cells by means of pressure injection. Pressure injection, with this experimental design, can not be used in these cell cultures. An overwhelming amount of pressure was required before an electrode could pass the HRP solution and electrode creep often became a significant problem. This meant that cells required holding for periods longer than 30 minutes as opposed to the 5 to 10 minute period needed for cells injected electrophoretically. Because HRP solution can not

been seen in the medium it was not possible to determine if the HRP solution had reached the tip of the electrode.

An interesting observation from this study was the characteristically low resting membrane potential of the cells that were injected, and the relatively short period of time that they were held. Initially, it was assumed that it would be optimal and almost necessary to hold these cells for periods of at least thirty minutes and that they would need to have resting membrane potentials of at least -60 mv for transport to be successful. Of the 30 neurons included as data, most were held for only 5 to 10 minutes and displayed resting membrane potentials of only -15 to -25 mv during injection. These cells most likely had normal resting potentials but were injured upon impalement.

Another observation that was made during the course of this research was with regard to the glass microelectrodes used to impale neurons. Prior to the study, an impression was given that electrodes suitable for use would necessitate tips of less than 0.1 μm in diameter and display impedances of 100 to 120 μV. It was my experience that tip configuration was the most important factor when selecting an electrode. Electrodes with low impedances, 20 to 30 μV, but needlelike tips provided smooth, stable impalements while still allowing HRP passage.

APPENDIX

SINGLE NEURON RECONSTRUCTIONS

SINGLE NEURON RECONSTRUCTION
DATA CELL 1
DATE IMPALED 10/15/87
CULTURE DATE 9/17/87

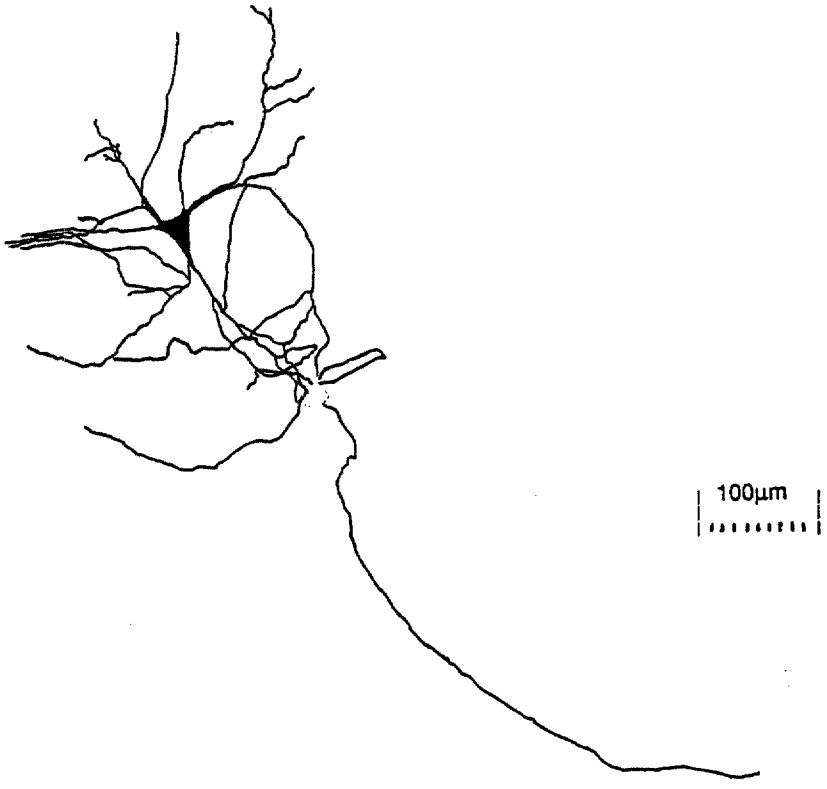

SINGLE NEURON RECONSTRUCTION
DATA CELL 2
DATE IMPALED 10/15/87
CULTURE DATE 9/17/87

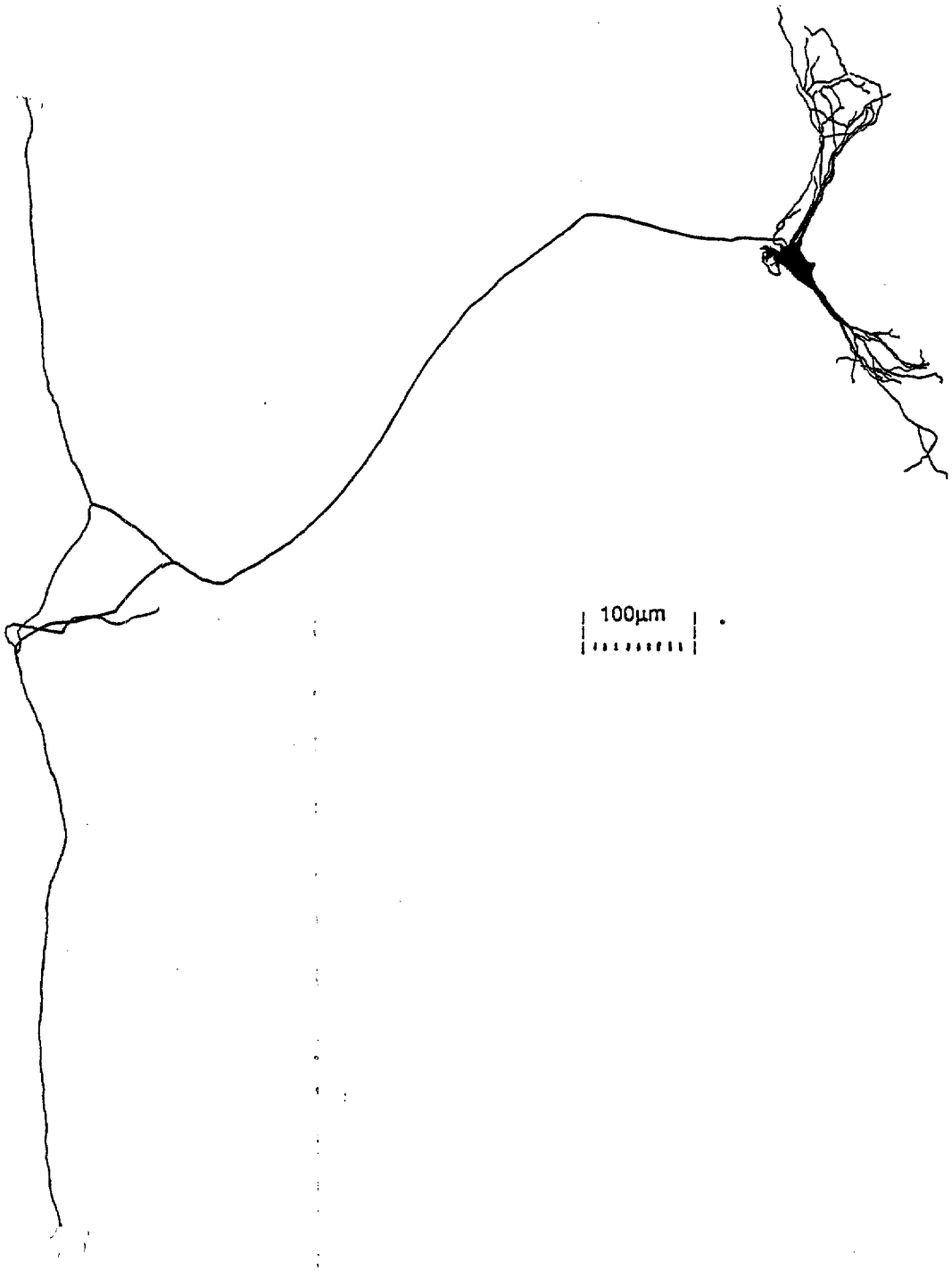

SINGLE NEURON RECONSTRUCTION

DATA CELL 3
DATE IMPALED 1/19/88
CULTURE DATE 12/22/87

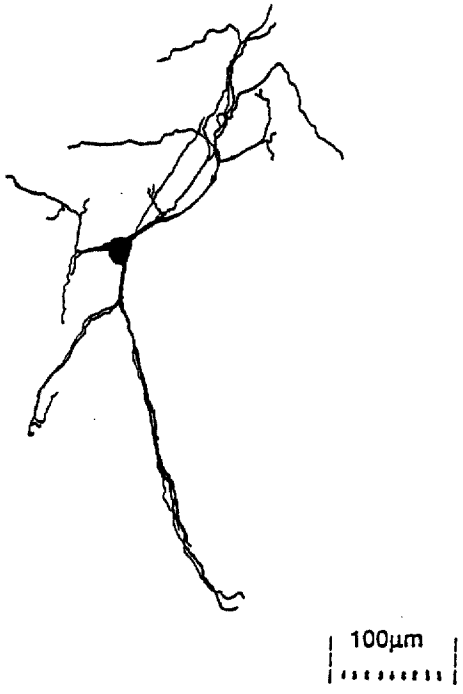

SINGLE NEURON RECONSTRUCTION
DATA CELL 4
DATE IMPALED 1/19/88
CULTURE DATE 12/22/87

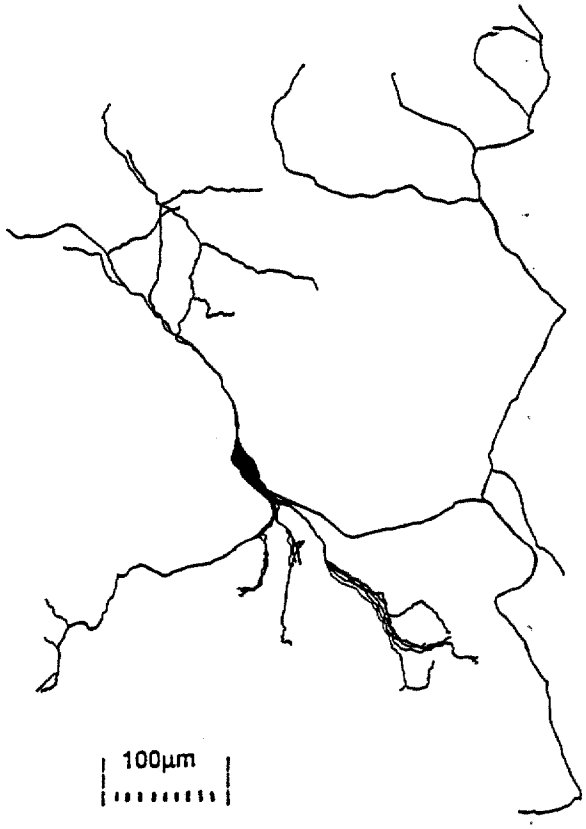

SINGLE NEURON RECONSTRUCTION
DATA CELL 5
DATE IMPALED 1/25/88
CULTURE DATE 12/22/87

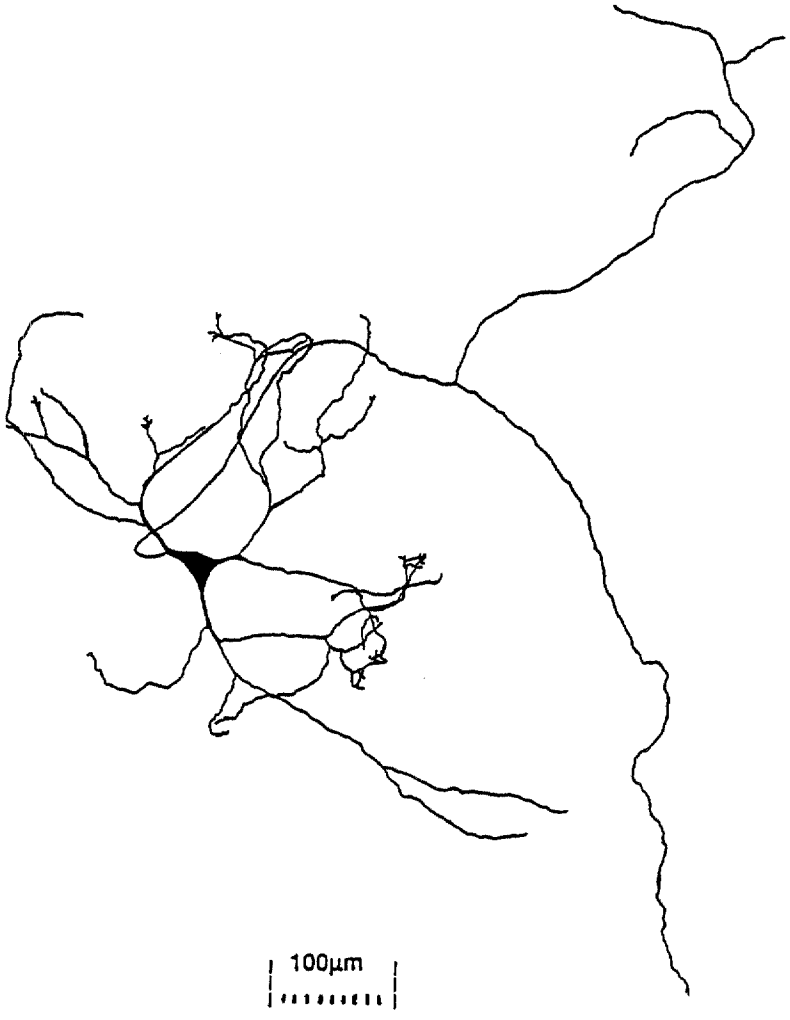

SINGLE NEURON RECONSTRUCTION
DATA CELL 6
DATE IMPALED 1/25/88
CULTURE DATE 12/22/87

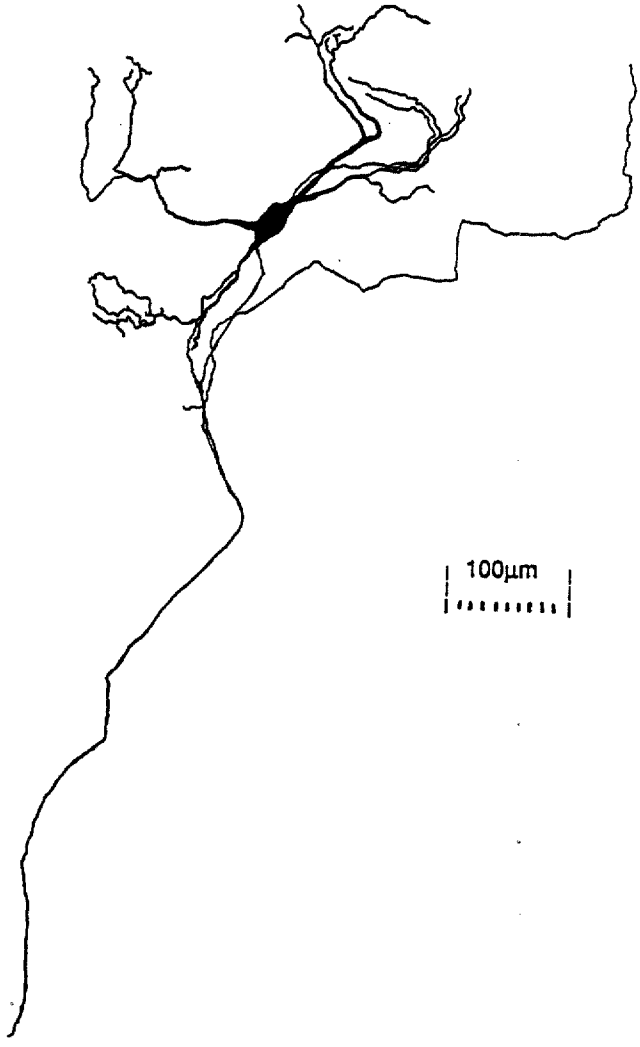

SINGLE NEURON RECONSTRUCTION
DATA CELL 7
DATE IMPALED 1/25/88
CULTURE DATE 12/22/87

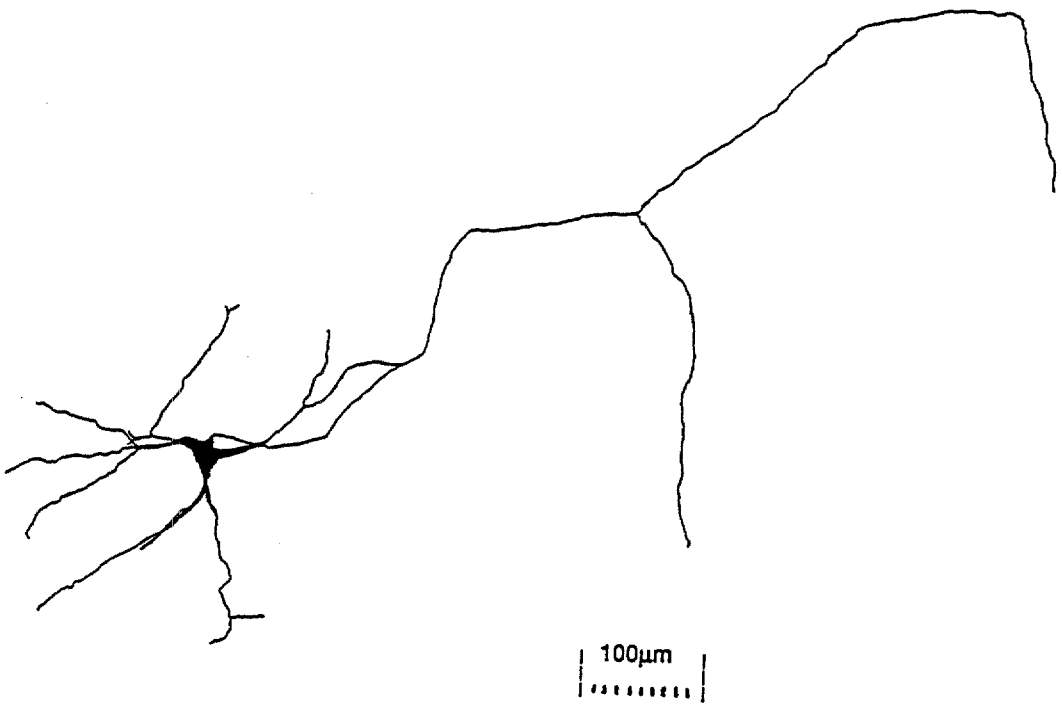

SINGLE NEURON RECONSTRUCTION
DATA CELL 8
DATE IMPALED 2/11/88
CULTURE DATE 1/14/88

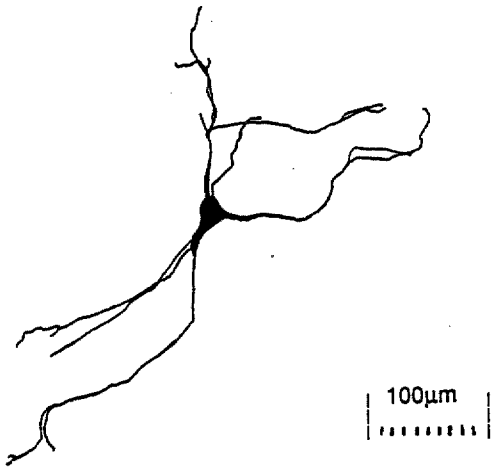

SINGLE NEURON RECONSTRUCTION
DATA CELL 9
DATE IMPALED 2/11/88
CULTURE DATE 1/14/88

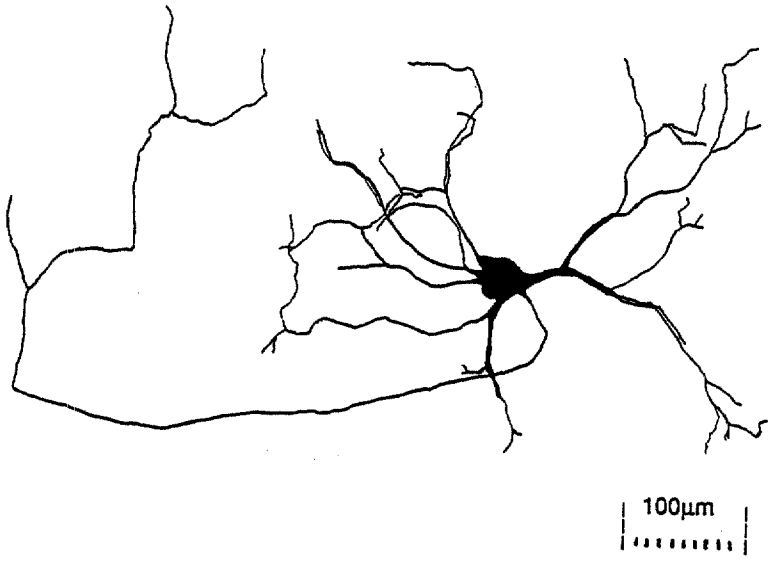

SINGLE NEURON RECONSTRUCTION
DATA CELL 10
DATE IMPALED 2/11/88
CULTURE DATE 1/14/88

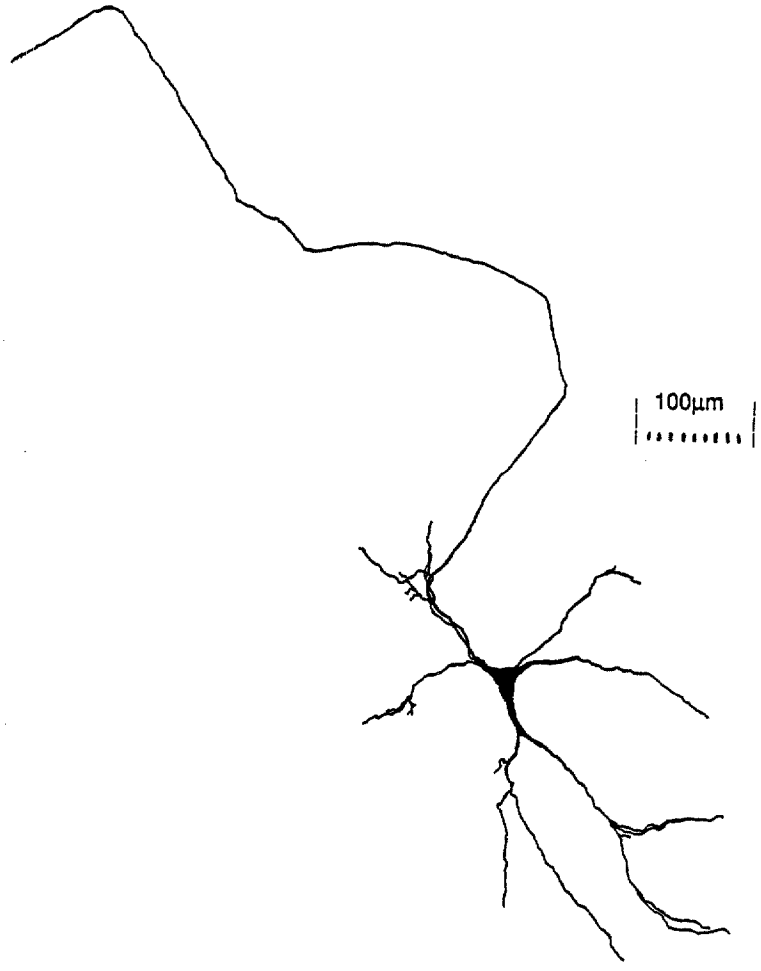

SINGLE NEURON RECONSTRUCTION
DATA CELL 11
DATE IMPALED 2/17/88
CULTURE DATE 1/14/88

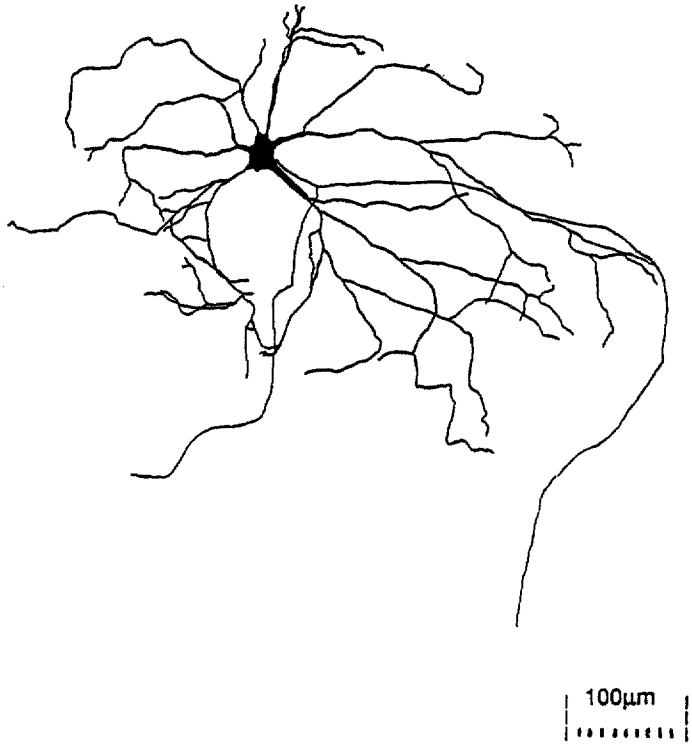

SINGLE NEURON RECONSTRUCTION
DATA CELL 12
DATE IMPALED 2/17/88
CULTURE DATE 1/14/88

SINGLE NEURON RECONSTRUCTION
DATA CELL 13
DATE IMPALED 2/17/88
CULTURE DATE 1/14/88

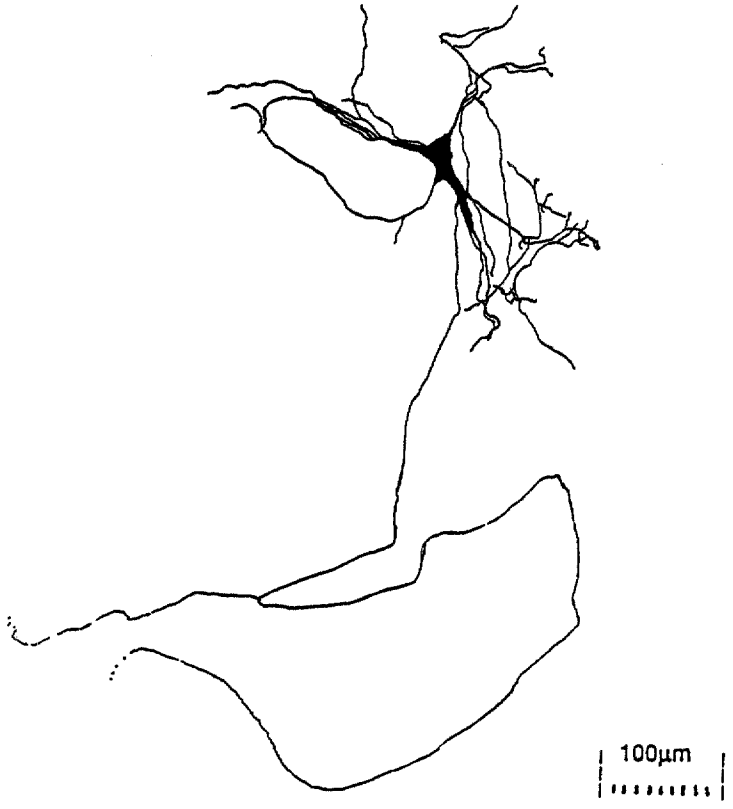

SINGLE NEURON RECONSTRUCTION
DATA CELL 14
DATE IMPALED 2/17/88
CULTURE DATE 1/14/88

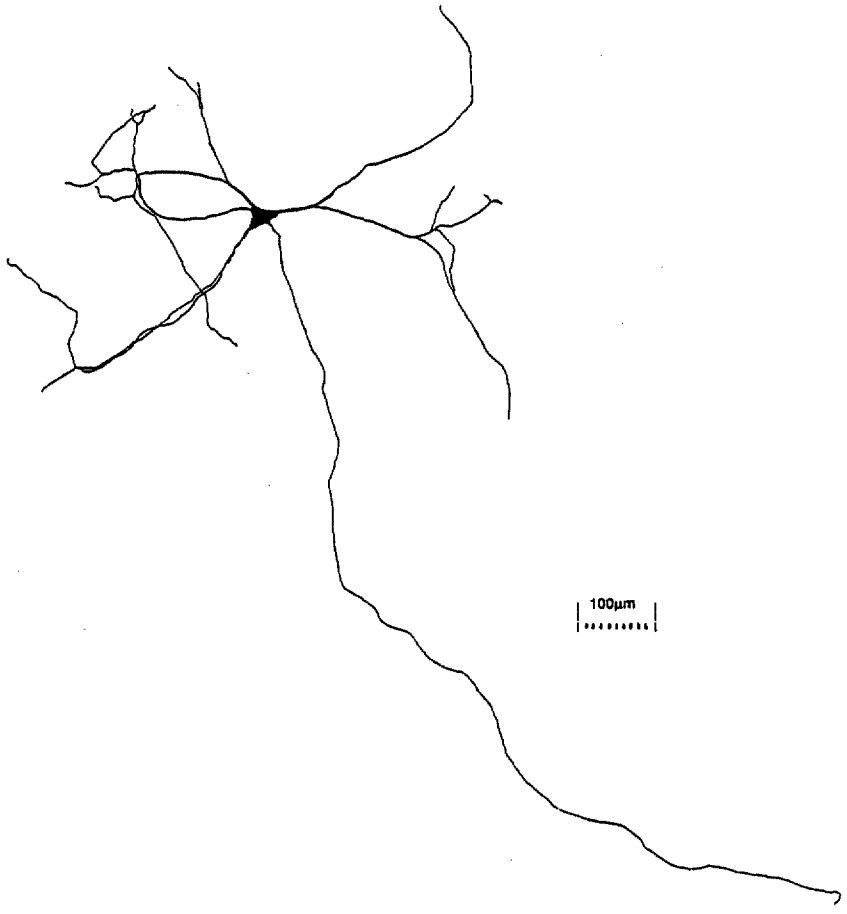

SINGLE NEURON RECONSTRUCTION
DATA CELL 15
DATE IMPALED 2/17/88
CULTURE DATE 1/14/88

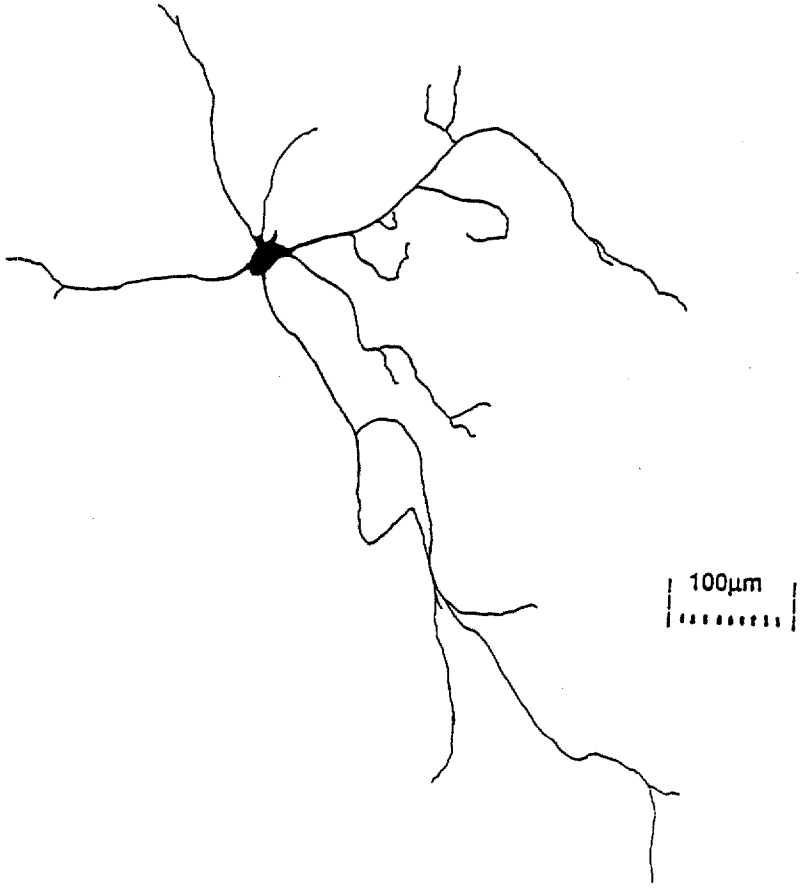

SINGLE NEURON RECONSTRUCTION
DATA CELL 16
DATE IMPALED 2/17/88
CULTURE DATE 1/14/88

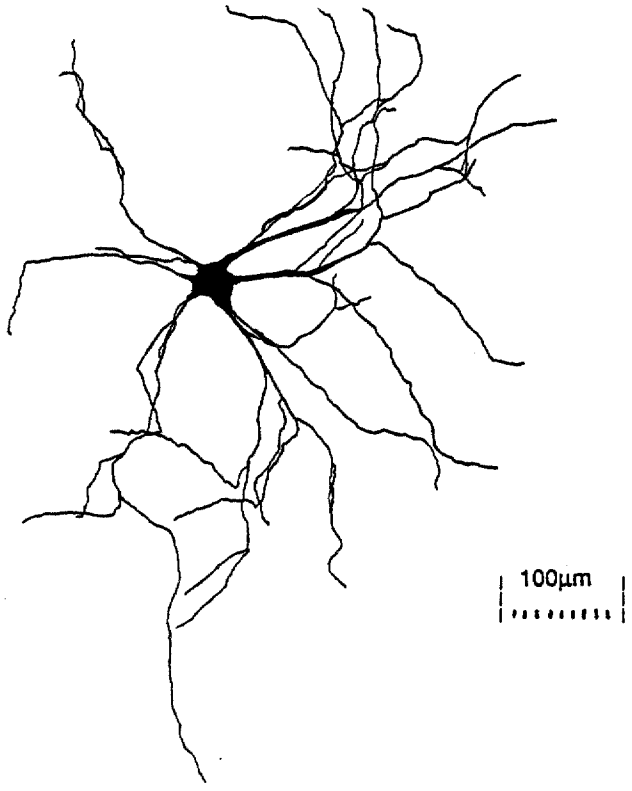

SINGLE NEURON RECONSTRUCTION
DATA CELL 17
DATE IMPALED 2/17/88
CULTURE DATE 1/14/88

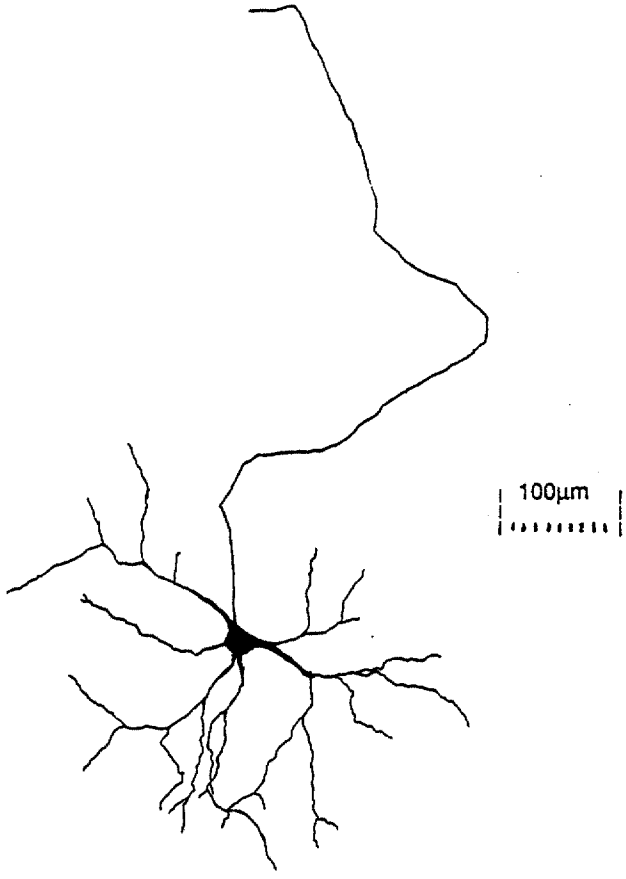

SINGLE NEURON RECONSTRUCTION
DATA CELL 18
DATE IMPALED 2/17/88
CULTURE DATE 1/14/88

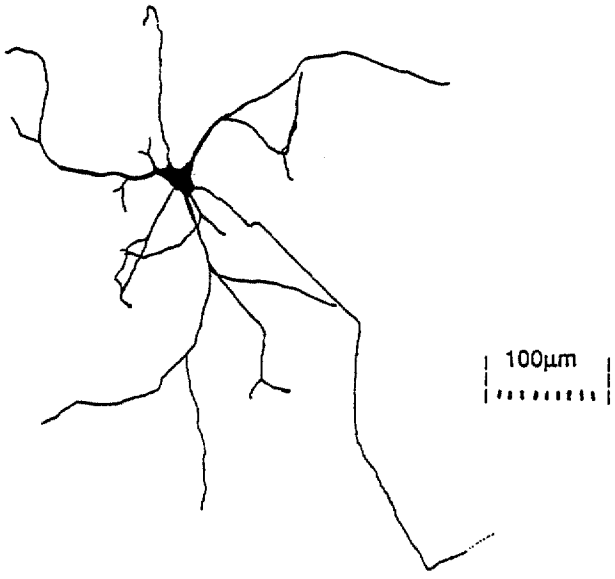

SINGLE NEURON RECONSTRUCTION
DATA CELL 19
DATE IMPALED 2/24/88
CULTURE DATE 1/21/88

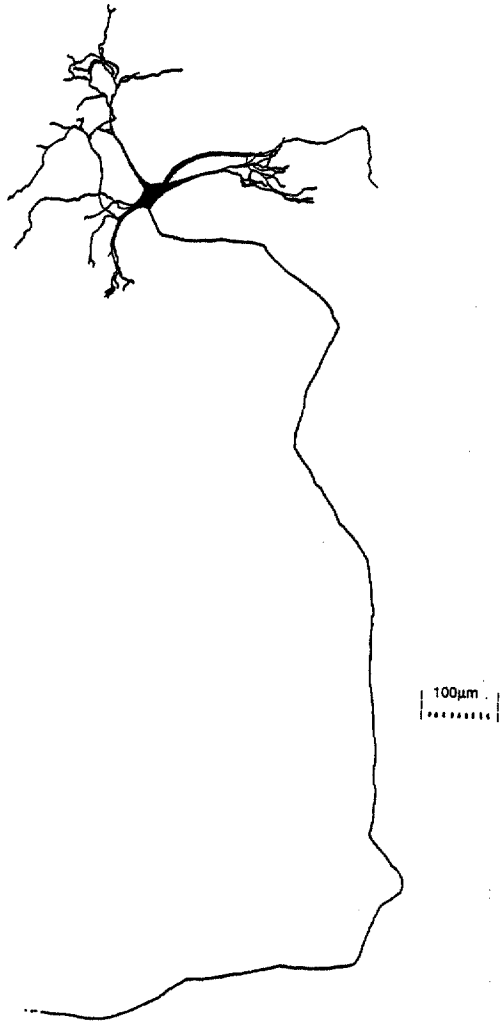

SINGLE NEURON RECONSTRUCTION
DATA CELL 20
DATE IMPALED 3/3/88
CULTURE DATE 1/28/88

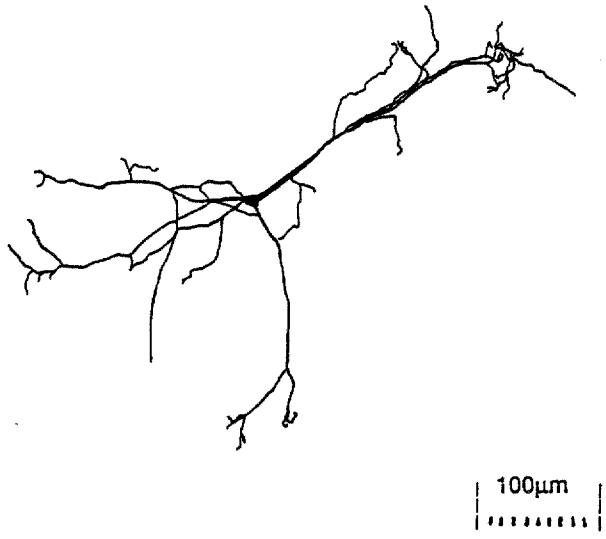

SINGLE NEURON RECONSTRUCTION
DATA CELL 21
DATE IMPALED 3/31/88
CULTURE DATE 3/3/88

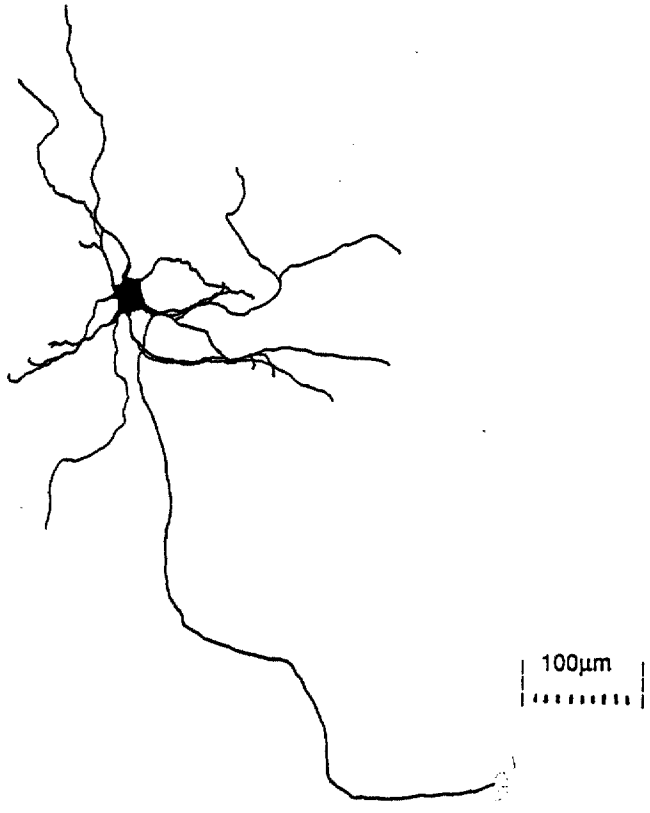

SINGLE NEURON RECONSTRUCTION
DATA CELL 22
DATE IMPALED 3/31/88
CULTURE DATE 3/3/88

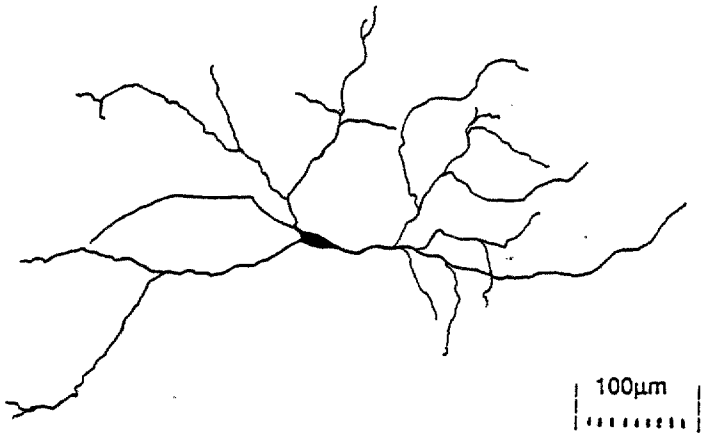

SINGLE NEURON RECONSTRUCTION
DATA CELL 23
DATE IMPALED 3/31/88
CULTURE DATE 3/3/88

SINGLE NEURON RECONSTRUCTION
DATA CELL 24
DATE IMPALED 6/13/88
CULTURE DATE 5/11/88

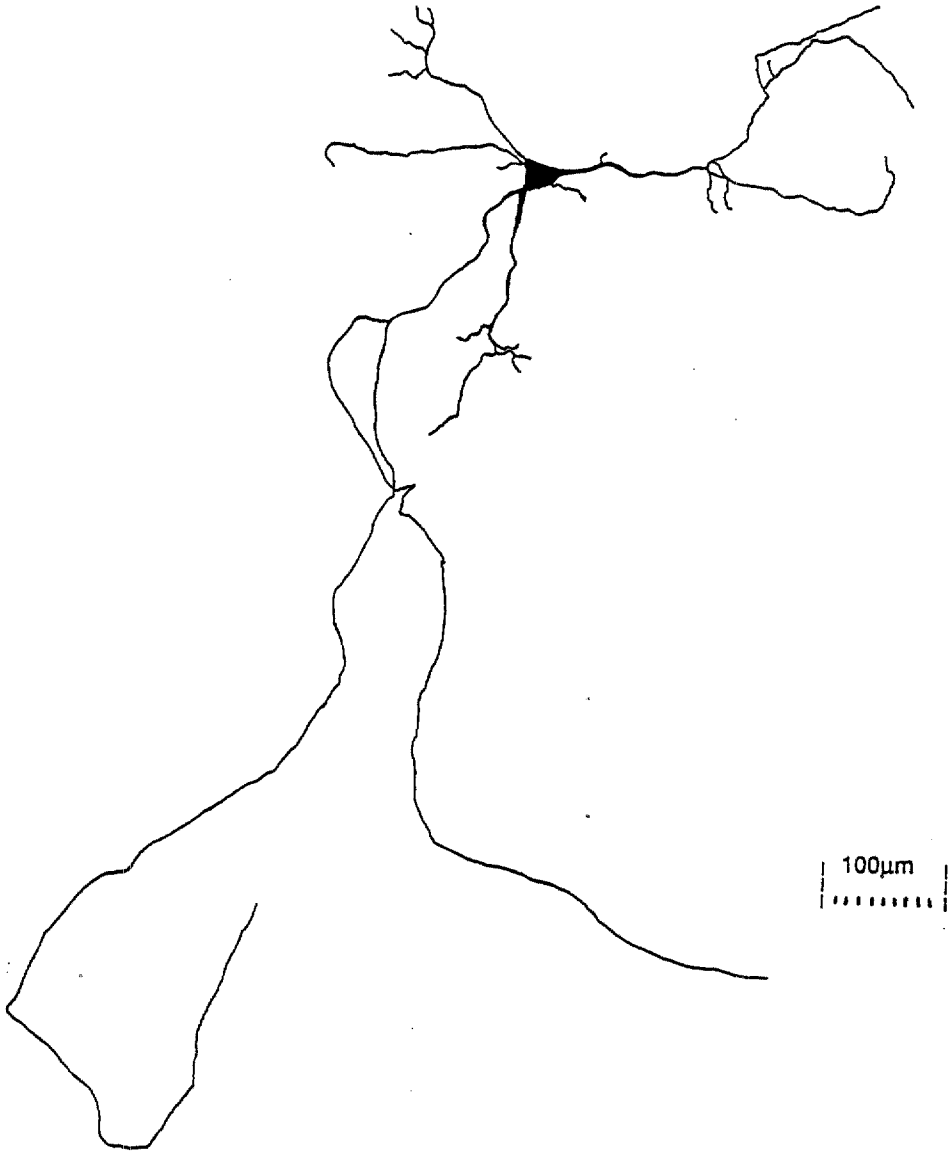

SINGLE NEURON RECONSTRUCTION
DATA CELL 25
DATE IMPALED 6/13/88
CULTURE DATE 5/11/88

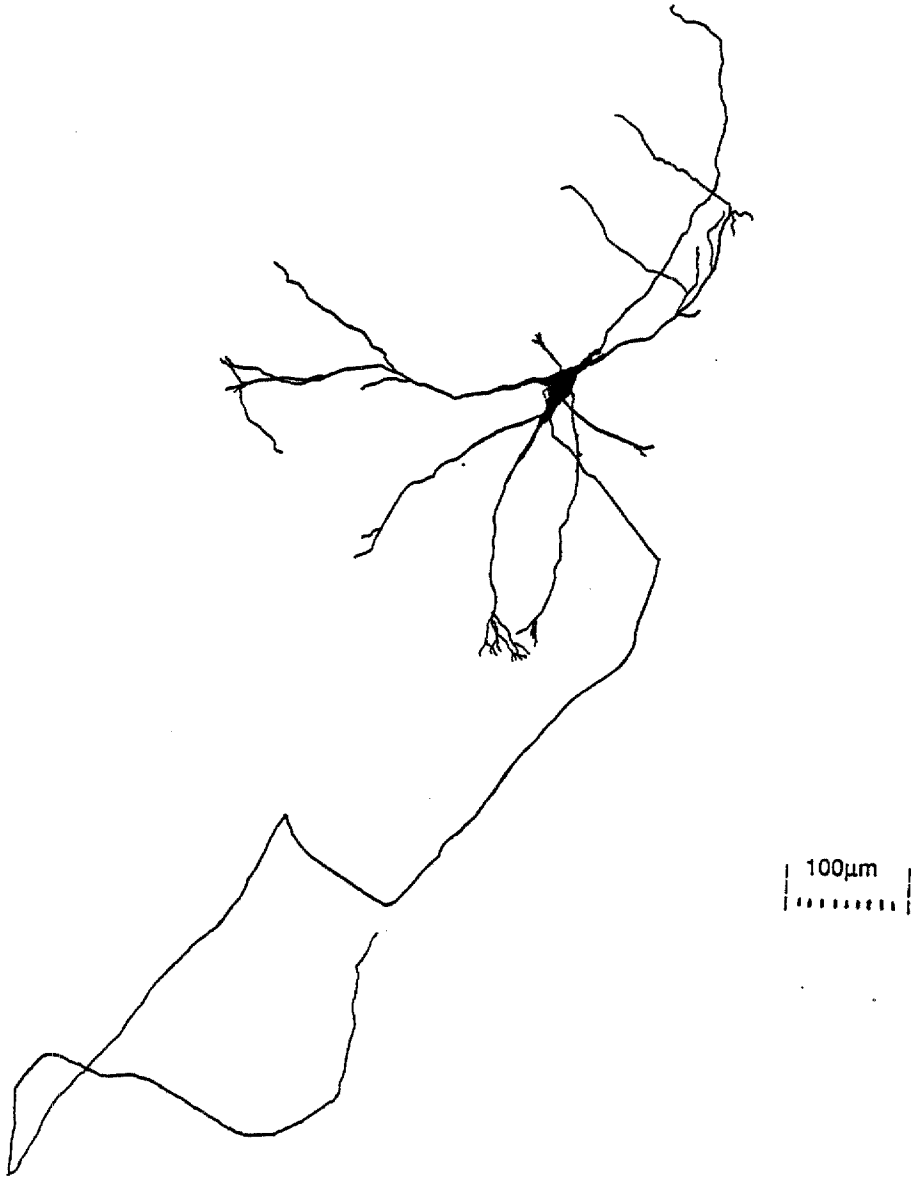

SINGLE NEURON RECONSTRUCTION
DATA CELL 26
DATE IMPALED 6/13/88
CULTURE DATE 5/11/88

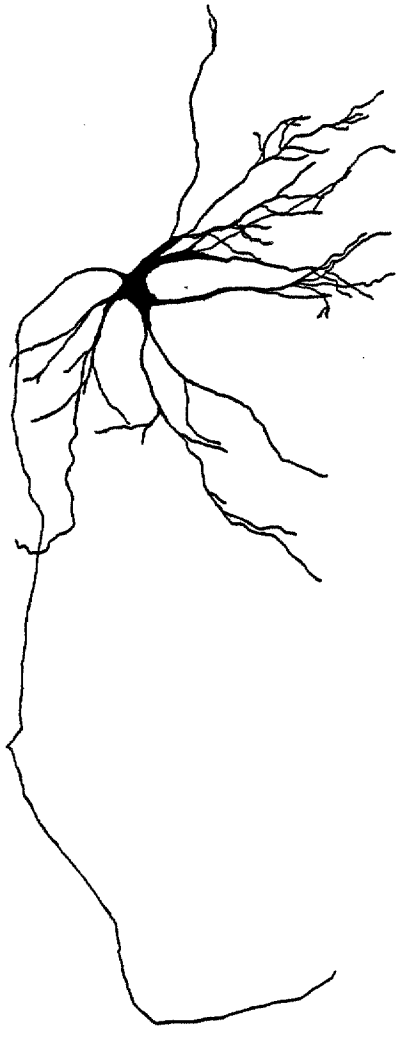

SINGLE NEURON RECONSTRUCTION
DATA CELL 27
DATE IMPALED 6/16/88
CULTURE DATE 5/11/88

SINGLE NEURON RECONSTRUCTION
DATA CELL 28
DATE IMPALED 6/16/88
CULTURE DATE 5/11/88

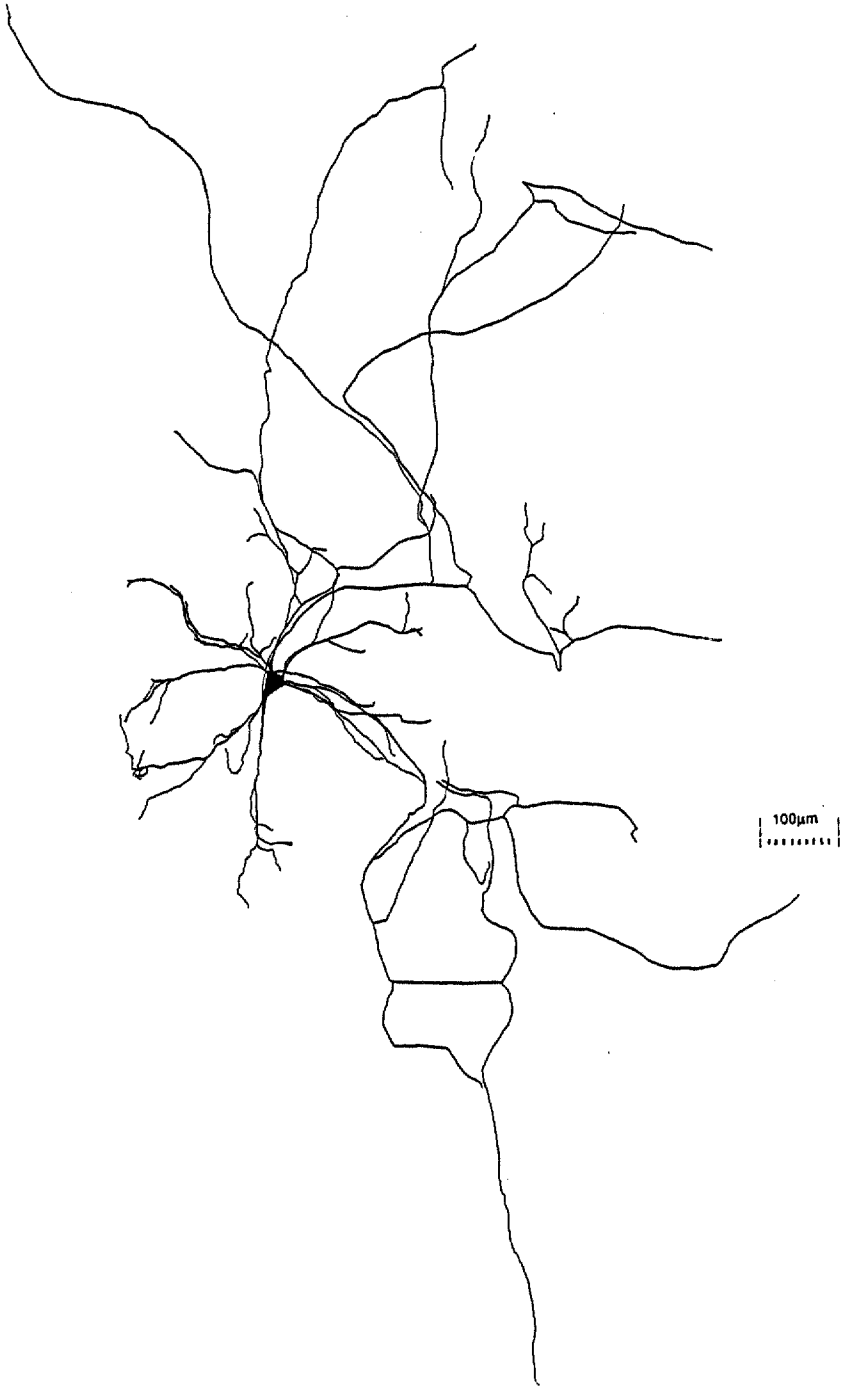

SINGLE NEURON RECONSTRUCTION
DATA CELL 29
DATE IMPALED 6/16/88
CULTURE DATE 5/11/88

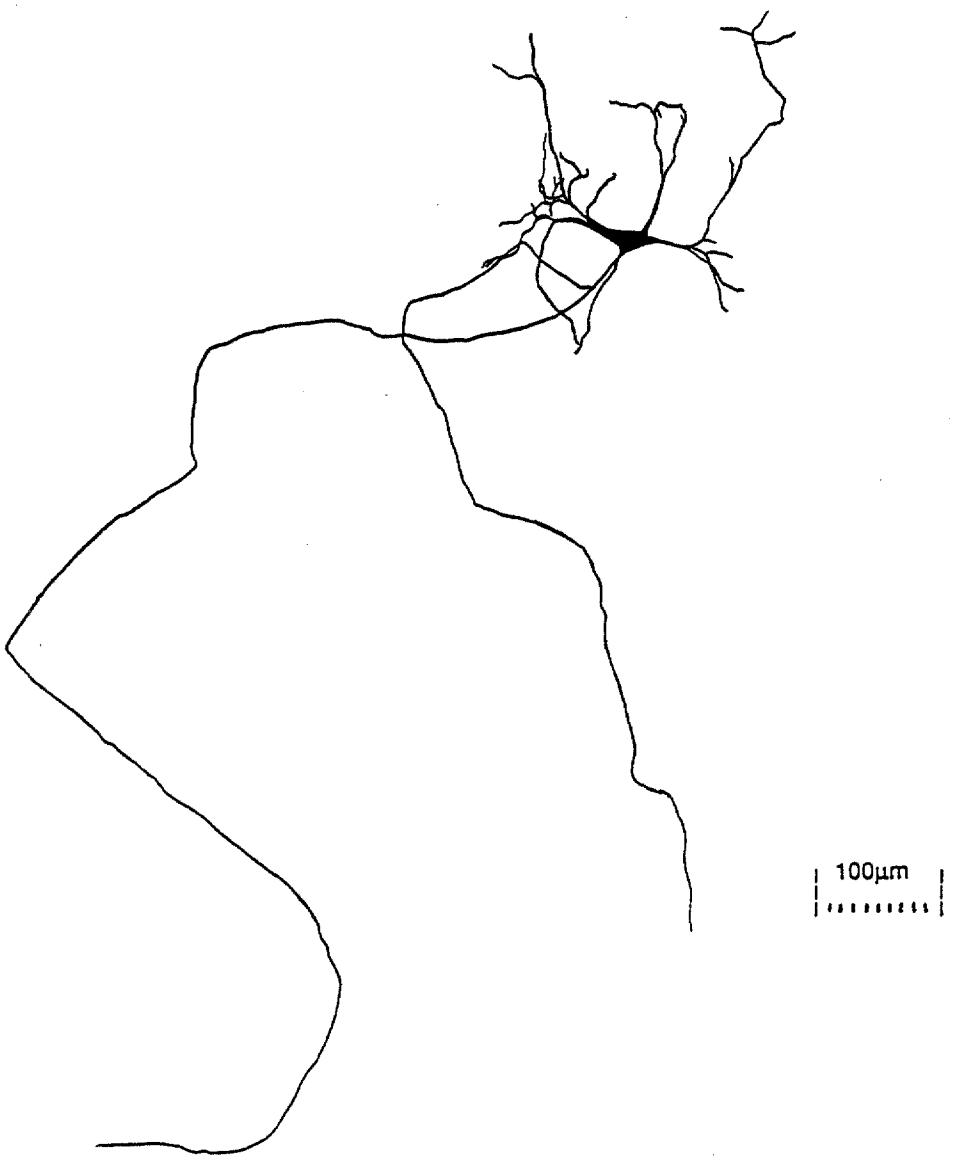

SINGLE NEURON RECONSTRUCTION
DATA CELL 30
DATE IMPALED 2/24/88
CULTURE DATE 1/21/88

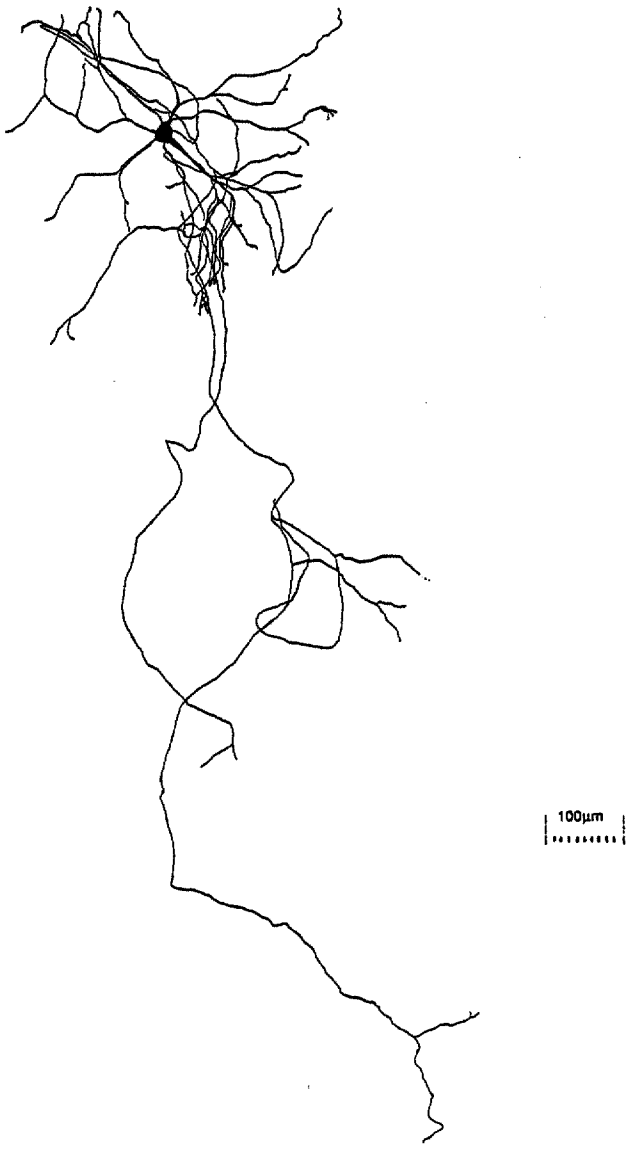

LITERATURE CITED

Bishop, G. A., H. T. Chang, and S. T. Kitai. 1979a. Light and electron microscopic analysis of various neostriatal neurons intracellularly labelled with HRP. II. Patterns of axonal distribution. Soc. For Neurosci. Absts. 6: 470.

Bishop, G. A., J. S. King, and R. A. McCrea. 1980a. Light and electron microscopic analysis of purkinje cell axon collaterals. An intracellular horseradish peroxidase study in the cat. Soc. for Neurosi. Absts. 11: 135.

Bishop, G. A., R. A. McCrea, and J. S. King. 1980b. An analysis of the morphology and cytology of HRP labelled purkinje cells. Brain Res. Bull. 5: 563-574.

Bishop, G. A., and J. S. King. Intracellular horseradish peroxidase injections for tracing neural connections. 1982. In Tracing neural connections with horseradish peroxidase. ed. M-M Mesulam, 185-242. Singapore. Wiley & Sons.

Bowman, M. H., and J. S. King. 1973. The conformation, cytology, and synaptology of the opossum inferior olivary nucleus. J. comp. Neurol. 148: 491-524.

Brightman, M. W. 1965. The distribution within the brain of ferritin injected into cerebrospinal fluid compartments. J. Cell. Biol. 26: 99-123.

Broadwell, R. D., and M. W. Brightman. 1979. Cytochemistry of undamaged neurons transporting exogenous protein *in vivo*. J. comp. Neurol. 185: 31-74.

Brown, A. G., and R. E. W. Fyffe. 1981. Direct observations on the contacts made between Ia afferent fibers and alpha-motorneurons in the cat's lumbosacral spinal cord. J. Physiol. 313: 121-140.

Chan-Palay, V. 1971. The recurrent collaterals of purkinje cell axons: A correlated study of the rat's cerebellar cortex with electron microscopy and the Golgi method, Z. anat. Entwickl-Gesch. 134: 200-234.

Chan-Palay, V. 1977. Cerebellar dentate nucleus organization, cytology and transmitters. Berlin-Heidelberg, New York. Springer-Verlag.

Chang, H. T., C. Wilson, and S. T. Kitai. 1980. Collateral arborization of axons of rat striatal neurons in the rat globus pallidus studied by intracellular horseradish peroxidase labelling. Soc. For Neurosci. Absts. 6: 269.

Christensen, B. N., and F. E. Ebner. 1978. The synaptic architecture of neurons in opossum somatic sensory-motor cortex: a combined anatomical and physiological study. J. Neurocytol. 7: 39-60.

Cullheim, S., and J-O. Kellereth. 1976. Combined light and electron microscopic tracing of neurons, including axons and synaptic terminals, after intracellular injection of horseradish peroxidase. Neurosci. Lett. 2: 307-313.

Cullheim, S., J-O. Kellereth, and S. Conradi. 1977. Evidence for direct synaptic interconnections between cat spinal alpha motorneurons via the recurrent axon collaterals: a morphological study using intracellular injection of HRP. Brain Res. 132: 1-10.

Deniau, J. M., I. Grofova, D. Steindler, and S. T. Kitai. 1980. Axonal arborizations of nigrothalamic and nigrotectal cells: anatomical and electrophysiological studies. Soc. for Neurosci. Absts. 6: 807.

DiFiglia, M., P. Pasik, and T. Pasik. 1976. A Golgi study of neuronal types in the neostriatum of monkeys. Brain Res. 114: 245-256.

Fox, C. A., A. A. Andrade, D. E. Hillman, and R. Schwynn, (1971/1972a). The aspiny neurons and the glia in the primate striatum. J. Hirnforsch. 13: 181-201.

Fox, C. A., D. E. Hillman, K. A.Siegesmund, and C. R. Dutta 1967. The primate cerebellar cortex: a Golgi and electron microscopic study. Prog. Brain Res. 25: 174-225.

Geisert, E. E., Jr. 1976. The use of tritiated horseradish peroxidase for defining neuronal pathways: a new application. Brain Res. 117: 130-135.

Gillete, R., and B. Pomeranz. 1973a. Neuron geometry and circuitry via the electron microscope: intracellular staining with an osmiophillic polymer. Science. 182: 1256-1258.

Gobel, S., W. M. Falls, G. S. Bennett, M. Abdelmmoumene, H. Hayashi, and E. Humphrey. 1980. An electron microscopic analysis of the synaptic connections of HRP filled stalk cells and islet cells in the substantia gelatinosa of adult cat spinal cord. J. Comp. Neurol. 194: 781-808.

Graham, R. C. Jr., and M. J. Karnovsky. 1966. The early stages of absorption of injected horseradish peroxidase in the proximal tubules of mouse kidney: ultrastructural cytochemistry by a new technique. J. Histochem. Cytochem. 14: 291-302.

Graybiel, A. M., and M. Devor. 1974. A microelectrophoretic delivery technique for use with horseradish peroxidase. Brain Res. 68: 167-173.

Gross, G. W., and J. H. Lucas. 1982. Long term monitoring of spontaneous single unit activity from neuronal monolayer networks cultured on photoetched multielectrode surfaces. J. Electrophysiol. Tech. 9: 55-67.

Gross, G. W., and M. H. Hightower. 1987. Multielectrode investigations of network properties in neuronal monolayer cultures. In Precedings of the Sixth Southern Biomedical Engineering Conference. 212-217. Washington D.C. McGregor and Werner.

Gwynn, D. G., G. P. Nicholson, and B.A. Flumerfelt. 1977. The inferior olivary nucleus of the rat: a light and electron microscopic study. J. comp. Neurol. 174: 489-520.

Hanker, J. S., J. J. Nordem, R. W. Oppenheim, and I. T. Diamond. 1976. Design and characterization of fluorochrome-conjugated horseradish peroxidases for neuronal tracing. Neurosci. Abstr. 2: 37.

Horwitz, B. 1981. Beyond the 3/2 rule: Unequal lengths and diameters and their effects on transient voltages in neurons with branching dendritic trees. Soc. Neurosci. Abstr. 7: 360.

Jankowska, E., J. Rastad, and J. Westman. 1976. Intracellular application of horseradish peroxidase and its light and electron microscopic appearance in spinocervical tract cells. Brain Res. 105: 557-562.

Jarvilehto, M., I. A. Meinertzhagen, and S. R. Shaw. 1986. Anti-adhesive coating for glass microelectrodes. Journal of Neurosci. Methods. 17: 327-334.

Kemp, J. M., and T. P. S. Powell. 1971. The structure of the caudate nucleus of the cat: Light and electron microscopy. Phil. Trans. Roy. Soc. Lond. B. 262: 383-401.

Kim, C. C., and P. L. Strick. 1976. Critical factors involved in the demonstration of horseradish peroxidase retrograde transport. Brain Res. 103: 356-361.

King, J. S., and R. A. McCrea. 1978. A cytological analysis of inferior olivary neurons after intracellular injections of horseradish peroxidase. Anat. Rec. 190: 446.

Kitai, S. T., J. D. Kocsis, R. J. Preston, and M. Sugimori. 1976. Monosynaptic inputs to caudate neurons identified by intracellular injection of horseradish peroxidase. Brain Res. 118: 132-136.

Kristensson, K., and Y. Olsson. 1971. Retrograde axonal transport of protein. Brain Res. 29: 363-365.

La Vail, J. H., and M. M. LaVail. 1974. The retrograde intraaxonal transport of horseradish peroxidase in retinal ganglion cells of the chick. Brain Res. 85: 273-280.

LaVail, J. H., S. Rapisardi, and I. K. Sugin. 1980. Evidence against the smooth endoplasmic reticulum as a continuous channel for the retrograde axonal transport of horseradish peroxidase. Brain Res. 191: 3-20.

Litchy, W. J. 1973. Uptake and retrograde transport of horseradish peroxidase of frog sartorius nerve in vivo. Brain Res. 56: 377-381.

Lucas, J. H., G. W. Gross, D. G. Emery, and C. G. Gardner. 1985. Neuronal survival or death after dendrite transection close to the perikaryon: Correlation with electrophysiologic, morphologic, and ultrastructural changes. Central Nervous System Trauma 2: 231-255.

Lynch, G. S., R. L. Smith, P. Mensah, and C. Cotman. 1973. Tracing the mossy fiber system with horseradish peroxidase histochemistry. Exp. Neurol. 40: 516-524.

Malmgren, L., and Y. Olsson. 1978. A sensitive method for histochemical demonstration of horseradish peroxidase in neurons following retrograde axonal transport. Brain Res. 148: 279-294.

Mason, C. A., and J. A. Robson. 1979. Morphology of retinogeniculate axons in the cat. Neuroscience 4: 79-98.

McCrea, R. A., G. A. Bishop, and S. T. Kitai. 1976. Intracellular staining of purkinje cells and their axons with horseradish peroxidase. Brain Res. 118: 132-136.

McCrea, R. A., G. A. Bishop, and S. T. Kitai. 1977. Morphological and electrophysiological characteristics of projection neurons in the nucleus interpositus of the cat cerebellum. J.comp. Neurol. 181: 397-419.

Mesulam, M-M. 1976. The blue reaction product in horseradish peroxidase neurohistochemistry: incubation parameters and visibility. J. Histochem. Cytochem. 24: 1273-1280.

Mesulam, M-M. 1982. Principles of horseradish peroxidase neurohistochemistry and their applications for tracing neural pathways - Axonal transport, enzyme histochemistry, and light microscopic analysis. In Tracing Neural Connections with Horseradish Peroxidase ed. M-M Mesulam, 1-135. Singapore. Wiley & Sons.

Mesulam, M-M., and E. J. Mufson. 1980. The rapid anterograde transport of horseradish peroxidase. Neurosci. 5: 1277-1286.

Mesulam, M-M., and D. L. Rosene. 1977. Differential sensitivity between blue and brown reaction procedures for HRP neurohistochemistry. Neurosci. Lett. 5: 7-14.

Mesulam, M-M., and D. L. Rosene. 1979. Sensitivity in horseradish peroxidase neurohistochemistry: a comparative and quantitative analysis of nine methods. J. Histochem. Cytochem. 27: 763-773.

Muller, K. J., and U. J. McMahan. 1976. The shapes of sensory and motor neurons and the distribution of their synapses in the ganglia of the leech: A study using intracellular injection of HRP. Proc. R. Soc. Lond. B. 194: 481-499.

Nahvi, M. J., C. D. Woody, E. Tzevelikos, and C. E.Ribak. 1980. Electrophysiologic characterization of morphologically identified neurons in the cerebellar cortex of awake cats. Exp. Neurol. 67: 368-376.

Nishino, H., T. Ono, K. Sasaki, A. Nishino, and K. Muramoto. 1979. Retrograde transport of horseradish peroxidase in sciatic nerve of rats and dystrophy mice. Neurosci. Lett. 14: 1-6.

Norden, J. J., R. W. Oppenheim, I. T. Diamond, and J. S. Hanker. 1976. Cellular uptake and neuronal retrograde transport of fluorochrome-conjugated horseradish peroxidases. Neurosci. Abstr. 2: 41.

Ochs, S., and R. M. Worth. 1978. Axoplasmic transport in normal and pathological systems. In Physiology and Pathobiology of Axons. ed. S. G. Waxman, 251-264. New York. Raven Press.

Palay, S., and Chan-Palay, V. 1974. Cerebellar Cortex: Cytology and Organization. New York-Heidelberg-Berlin. Springer-Verlag

Preston, R. J., G. A. Bishop, And S. T. Kitai. 1980. The rapid anterograde transport of horseradish peroxidase. Neurosci. 5: 1277-1286.

Rall, W. 1962. Theory of physiological properties of dendrites. Ann. N. Y. Acad. Sci. 96: 1071-1092.

Ramon y Cajal, S. 1911. Histologie du Systeme Nerveux de Homme et das vertebres. Maloine, Paris.

Ransom, B. R., E. Neale, M. Henkart, P. N. Bullock, and P. G. Nelson. 1977. Mouse spinal cord in cell culture. I. Morphological and intrinsic neuronal electrophysiological properties. J. Neurophysiol. 40; 1132-1150.

Ribak, C. E., C. D. Woody, M. J. Nahvi, and E. Tzebelikos. 1980. Ultrastructural identification of physiologically recorded neurons in the cat cerebellum. Exp. Neurol. 67: 372-390.

Robson, J. A., and C. A. Mason. 1979. The synaptic organization of terminals traced from individual labelled retino-geniculate axons in the cat. Neuroscience 4: 99-112.

Rosene, D. L., and M-M. Mesulam. 1978. Fixation variables in horseradish peroxidase neurohistochemistry. I.The effects of fixation time and perfusion procedures upon enzyme activity. J. Histochem. Cytochem. 26:28-39.

Sakai, H., and C. D. Woody. 1978. Sampling distribution of morphologically identified neurons of the coronal-pericruciate cortex of awake cats following intracellular injections of horseradish peroxidase. Brain Res. 152: 329-333.

Sakai, M., H. Sakai, and C. D. Woody. 1978. Intracellular staining of cortical neurons by pressure microinjection of horseradish peroxidase and recovery by core biopsy. Exp. Neurol. 58: 138-144.

Scheibel, M. E., and A. Scheibel. 1955. The inferior olive: a Golgi study. J. comp. Neurol. 102: 77-132.

Schwartz, J. H. 1979. Axonal transport: components, mechanisms and specificity. Ann. Rev. Neurosci. 2: 467-504.

Smith, D. S. 1971. On the significance of cross-bridges between microtubules and synaptic vesicles. Phil. Trans. Roy. Soc. Lond. B. 261: 395-405.

Snow, P. J., P. K. Rose, and A. G. Brown. 1976. Tracing axons and axon collaterals of spinal neurons using intracellular injection of horseradish peroxidase. Science. 191: 312-313.

Sofroniew, M. V., and U. Schrell. 1980. Hypothalamic neurons projecting to the rat caudal medulla oblongata, examined by immunoperoxidase staining of retrogradely transported horseradish peroxidase. Neurosci. Lett. 19: 257-263.

Somogyi, P., and A. D. Smith. 1979. Projection of neostriatal spiny neurons to the substantia nigra. Application of a combined Golgi staining and horseradish peroxidase transport procedure at both light and electron microscopic levels. Brain Res. 178: 3-15.

Streit, P., and J. C. Reubi. 1977. A new and sensitive staining method for axonally transported horseradish peroxidase (HRP) in the pigeon visual system. Brain Res. 126: 530-537.

Szekely, G. 1976. The morphology of motorneurons and dorsal root fibers in the frog's spinal cord. Brain Res. 103: 275-290.

Szekely, G., and B. Kosaras. 1976. Dendro-dendritic contacts between frog motorneurons shown with the cobalt labelling technique. Brain Res. 108: 194-198.

Teichberg, S., E. Holtzman, S. M. Crain, and E. R. Peterson. 1975. Circulation and turnover of synaptic vesicle membrane in cultures fetal mammalian spinal cord neurons. J. Cell. Biol. 67: 215-230.

Tscihita, S., and H. Ishikawa. 1980. The movement of membranous organelles in axons. Electron microscopic identification of anterogradely and retrogradely transported organelles. J. Cell Biol. 84: 513-530.

Turner, P. T., and A. B. Harris. 1974. Ultrastructure of exogenous peroxidase in cerebral cortex. Brain Res. 74: 305-326.

Vacca, L. L., S. L. Rosario, E. A. Zimmerman, P. Tomashefsky, P. Y. Ng, and K. C. Hsu. 1975. Application ofimmunoperoxidase techniques to localize horseradish peroxidase-tracer in the central nervous system. J. Histochem. Cytochem. 23: 208-215.

Waxman, S. G., and G. D. Pappas. 1969. Pinocytosis at postsynaptic membranes: electron microscopic evidence. Brain Res. 14: 240-244.

Zwaagastra, B., and D. Kernell. 1981. Sizes of soma and stem dendrites in intracellularly labelled alpha-motorneurons of the cat. Brain Res. 204: 295-309.